Interactive Decision Support System for Planning and Construction of Large-Scale Tunneling Projects

FINAL REPORT
March 2025

Submitted by:

Rita N. Sousa, Ph.D.[1]
Assistant Professor

Matthew J. Bandelt, Ph.D., P.E.[2]
Associate Professor

Shengfeng Huang[1]
Graduate Research Assistant

Ehsan Mehryaar[2]
Graduate Research Assistant

[1]Department of Civil, Environmental and Ocean Engineering
Charles V. Schaefer, Jr. School of Engineering and Science
Stevens Institute of Technology
Hoboken, NJ 07030

[2]John A. Reif, Jr. Department of Civil and Environmental Engineering
Newark College of Engineering
New Jersey Institute of Technology
University Heights, Newark, NJ 07102

External Project Manager
Benjamin Engle – Gateway Corporation

In cooperation with
Rutgers, The State University of New Jersey
And
U.S. Department of Transportation
Federal Highway Administration

Disclaimer Statement

The contents of this report reflect the views of the authors, who are responsible for the facts and the accuracy of the information presented herein. This document is disseminated under the sponsorship of the Department of Transportation, University Transportation Centers Program, in the interest of information exchange. The U.S. Government assumes no liability for the contents or use thereof.

The Center for Advanced Infrastructure and Transportation (CAIT) is a Regional UTC Consortium led by Rutgers, The State University. Members of the consortium are Atlantic Cape Community College, Columbia University, Cornell University, New Jersey Institute of Technology, Polytechnic University of Puerto Rico, Princeton University, Rowan University, SUNY - Farmingdale State College, and SUNY - University at Buffalo. The Center is funded by the U.S. Department of Transportation.

1. Report No. CAIT-UTC-REG56	2. Government Accession No.	3. Recipient's Catalog No.	
4. Title and Subtitle Interactive Decision Support System for Planning and Construction of Large-Scale Tunneling Projects		5. Report Date March 2025	
		6. Performing Organization Code CAIT/NJIT/Stevens Institute of Technology	
7. Author(s) Rita L. Sousa (https://orcid.org/0000-0002-0617-0356) Matthew Bandelt (https://orcid.org/0000-0001-6681-2376) Shengfeng Huang (https://orcid.org/ 0000-0002-4789-2080) Ehsan Mehryaar (https://orcid.org/0000-0002-1036-7987)		8. Performing Organization Report No. CAIT-UTC-REG56	
9. Performing Organization Name and Address New Jersey Institute of Technology University Heights, Newark, NJ 07102 Stevens Institute of Technology 1 Castle Point Ter, Hoboken, NJ 07030 ·		10. Work Unit No.	
		11. Contract or Grant No. 69A3551847102	
12. Sponsoring Agency Name and Address Center for Advanced Infrastructure and Transportation Rutgers, The State University of New Jersey 100 Brett Road Piscataway, NJ 08854		13. Type of Report and Period Covered Final Report July 1, 2021– March 31, 2025	
		14. Sponsoring Agency Code	
15. Supplementary Notes U.S. Department of Transportation/OST-R 1200 New Jersey Avenue, SE Washington, DC 20590-0001			
16. Abstract Major transportation infrastructure projects have a strong impact on the surrounding communities. Tunnels, particularly in urban areas, provide greater benefits than above-the-ground alternatives, when considering reduced congestion and associated pollution, reduced disruption to businesses, pedestrians, and traffic during construction, and during their entire life cycle. Unfortunately, many well-known large-scale transportation infrastructure projects, in particular those with tunnels, are associated with high construction cost overruns and delays. These issues are mostly a result of the uncertainties associated with subsurface construction. It is, therefore, critical to develop a decision support system to quantify risk and uncertainties in underground construction that can be used by designers and decision-makers. This project was proposed in the context of this comprehensive transportation systems planning effort and the need for integrated approaches that includes the consideration of uncertainties into the planning of large tunnel systems. The developed approach was demonstrated with an application to the planning of the Hudson tunnel project. The project addresses the specific issue of natural hazards or risk events during construction and puts them into the context of the entire transportation system. Also, and very importantly, the planning of transportation systems under consideration of natural hazards are an issue of worldwide interest and necessity.			
17. Key Words large-scale transportation Infrastructure, tunnels, decision support system, risk assessment		18. Distribution Statement	
19. Security Classification (of this report) Unclassified	20. Security Classification (of this page) Unclassified	21. No. of Pages 59	22. Price

Form DOT F 1700.7 (8-69)

Acknowledgements

The research team would like to acknowledge the support of this work from the Center for Advanced Infrastructure, Stevens Institute of Technology, and New Jersey Institute of Technology. Additionally, we would like to thank the Gateway Corporation for providing data used in this report and additional technical comments. The research team would like to express their gratitude to the Geomechanics Group at the Massachusetts Institute of Technology (MIT) for their valuable support and advice throughout the project and for providing us access to software DAT free of charge. In particular, we would like to extend our deepest appreciation to Professor Herbert Einstein for his unwavering guidance and assistance.

Table of Content

1 Introduction 1

1.1 Structure of Report 1

1.2 Problem Description 1

1.3 Research Objectives and Tasks Definitions 2

1.3.1 Research Objectives 2

1.3.2 Tasks definitions 2

2 Detailed Descriptions of Tasks 1 through 4 3

2.1 Task 1 Geologic and construction data collection 3

2.2 Task 2 Stochastic Geologic modeling 5

2.2.1 Artificial intelligence framework 6

2.3 Neural Network (NN) 7

2.3.1 Random search hyper-parameter tuning 8

2.3.2 Evaluation Metrics 10

2.3.3 Data Collection and Data Structure 10

2.3.4 Methodology 11

2.3.5 Results and Discussion 12

2.4 Task 3 Geohazard, Risk characterization, and quantification 18

2.5 Task 3.1 Customization of DAT for the Hudson Tunnel and risk quantification 18

2.5.1 Data processing and geologic profile 19

2.5.2 DAT geology input 19

2.5.3 Resource management 22

2.5.4 Tunnel construction 22

2.5.5 Risk Events 24

2.5.6 Results 26

2.5.7 Sensitivity analyses 29

2.6 Task 4 TBM advance rate prediction using machine learning (construction) 33

2.6.1 Brief data description 34
2.6.2 Feature Selection and Data preparation 35
2.6.3 ML algorithms 35
2.6.4 Modeling results and analysis 36
2.6.5 Analysis large AR and large residual errors 41
2.6.6 Validation against a different project 44
3 Collaborative Activities 46
4 Conclusions 46
5 Recommendations 47

List of Figures

Figure 1 Hudson Project: Preferred Alternative alignment 3
Figure 2 Geological profile at the Washington Bridge site. Image Credit: illustration by Charles P. Berkey, 1948. 4
Figure 3 Borehole location within the research area 6
Figure 4 Simple Neural Network structure [4] 8
Figure 2 Random search hyperparameter tuning selection of points for two hyperparameter subspaces including one important and one unimportant variable [8] 9
Figure 3 Developing the model Process 11
Figure 4 Predicted soil profile versus observed soil profile at one borehole by Random Forest model 12
Figure 5 Accuracy of Random Forest model for each borehole 13
Figure 6 Predicted soil profile versus observed soil profile in one borehole using the Neural Network model 14
Figure 7 Accuracy of Neural Network model for each borehole 14
Figure 8 Division of each borehole log for boundary effect analysis 16
Figure 9 Division of the tunnel to various sections for geological complexity and borehole density analysis [13] 17
Figure 13 Research area 18
Figure 14 geology conditions of the Hudson River Tunnel 19
Figure 15 Areas and Zones of the Hudson Tunnel (DAT input) 20
Figure 16 Ground classes used in the Hudson Tunnel study. 21
Figure 17 Tunnel network 23
Figure 18 Cost-time scattergram results of different flooding scenarios 27
Figure 19 ailed cost and time for different zones of the Hudson tunnel 28
Figure 20 Time vs Position (Hudson Tunnel) 28
Figure 21 Stock vs Position (Hudson Tunnel) 29
Figure 22 Sensitivity analysis on the number of water inflow occurrences 30
Figure 23 Sensitivity analysis of small water inflow proportion 31
Figure 24 Sensitivity analysis of delay and additional cost 32
Figure 25 Sensitivity analysis of increased cost and decreased advance rate 33
Figure 26 Plan view of Porto light metro project in Porto, Portugal 34
Figure 27 Performance of five different ML algorithms 38
Figure 28 Predicted AR, monitored AR, and residual errors over rings 40
Figure 29 Residual error distribution of five machine learning algorithms 41
Figure 30 Distribution of features and label over ring 384 43
Figure 31 Distribution of features and label over ring 42 44
Figure 32 Residual error distribution of five ML algorithms 46

List of Tables

Table 1 Hyper-parameter space for Random Forest and Neural Network models 9
Table 2 Performance metrics of Random Forest model for base scenario 12
Table 3 Performance metrics of the Neural Network model for the base scenario 13
Table 4 Effect of data extraction distance on performance of the models 15
Table 5 Effect of number of borehole data used for training the model on performance of the model 15
Table 6 Performance of the models with and without borehole tips 16
Table 7 Performance of the models developed in different sections of the tunnels 17
Table 8 Zones definition in the DAT using probabilistic and deterministic E.P. definitions 21
Table 9 Geometry parameters of tunnel and shaft 23
Table 10 Cost and time for different categories 24
Table 11 Water inflow treatment methods description 25
Table 12 Delay and additional cost for method change to simulate the consequences of a catastrophic flood event (triangular probability distribution) 25
Table 13 Advance rate and unit cost associated with small water inflow (triangular probability distribution) 25
Table 14 Delay and Additional Cost induced by water inflow 27
Table 15 cases of additional cost and delay investigated in the sensitivity analysis 31
Table 16 Variance of additional cost and delay 32
Table 17 Performance of five different machine learning algorithms 36

1 Introduction

1.1 Structure of Report

This report will, in the remainder of the introduction, provide information on the background and problem description, the project objective, and the modified objectives and task descriptions. The main part - Section 2 - will describe the research methodology and findings structured by tasks. The conclusions and recommendations are provided in Sections 4 and 5, respectively.

1.2 Problem Description

The integration of urban and transportation systems in cities is essential to ensure their efficient planning, implementation, and operation. However, these systems are complex and comprise several subsystems that interact during construction and operation, leading to spatial and temporal uncertainties that affect their performance. To address this issue, this research project aimed to analyze the effects of uncertainty on urban and transportation systems and develop a comprehensive set of integrated methods and tools to account for natural geological uncertainties. The primary objective of this research was to provide a framework that could be extended to other natural hazards, aiding in decision-making processes related to urban and transportation systems. The study aimed to identify and analyze the sources of uncertainty in these systems and develop methods and tools to integrate uncertainty analysis into decision-making processes. This was done through the application of the developed methodologies to the case study of the new Hudson tunnel, The final goal was to provide planners, designers, and decision-makers with an approach to account for natural geological uncertainties in urban and transportation systems, ultimately contributing to the development of more efficient and resilient cities.

This research supports the USDOT strategic goals, particularly in the "Infrastructure" and "Innovation" areas described in the "USDOT Strategic Plan FY 2018-2022" as follows:

INFRASTRUCTURE: This strategic goal calls for the "Investment in Infrastructure to Stimulate Economic Growth, Productivity and Competitiveness for American Workers and Businesses." The research developed a decision aid tool to help guide investments that stimulate economic growth, such as the cost-efficient construction of underground infrastructure, enabling efficient and safe movement of people and goods. The developed integrated interactive decision support system developed can local and regional agencies, as well as private design companies, to leverage Federal funding (the proposed research was applied to the Gateway Tunnel, which Federal funds will partially support), accelerate project delivery, and reduce project life-cycle costs.

INNOVATION: This USDOT strategic goal targets the "Development and Deployment of Innovative Practices and Technologies that Improve the Performance of the US Transportation System". While the developed decision support system was initially tested and demonstrated using the Gateway Tunnel project data, it may potentially be employed in other major underground infrastructure projects. The approach itself was developed as an innovative practice that aims at leveraging the financial, human, and equipment resources in the construction and maintenance of underground infrastructure.

1.3 Research Objectives and Tasks Definitions

1.3.1 Research Objectives

The goal of the project is to increase safety and minimize the risks of major underground infrastructure systems by enhancing existing methods for stochastic subsurface characterization, hazard, and risk assessment. The specific objectives of the project are to develop a framework for large-scale tunneling projects capable of (1) Stochastic modeling of the subsurface to quantify the effects of subsurface uncertainties on tunnel construction costs and times, (2) determining most likely hazards along a tunnel, route for identification of 'risky' spots along tunnel alignment (3) performing quantitative risk assessment during the design and construction phases.

1.3.2 Tasks definitions

The following work plan was carried out in coordination with the stakeholders to achieve project goals and objectives:

TASK 1 - Geologic and construction data collection

Available geologic and construction data collected on the Hudson tunnel in collaboration with Gateway Corporation. The collected data was used to develop a geologic model for the Hudson tunnel alignment and determine probability distribution functions for input parameters of the next tasks.

TASK 2 – Stochastic Geologic modeling

This task included Stochastic 3D geologic modeling framework and algorithms will be developed to characterize uncertainties related to the subsurface. To test the framework, this task will make use of the geologic and construction data collected in Task 1. Specifically, Machine learning based model was developed to 3D geologic based on borehole data. The Models were used to predict lithology of the ground associated to a section of the Hudson Tunnel Project. Data sources for developing the model include 63 excavated boreholes along the proposed tunnel path.

TASK 3 – Planning phase: Geohazard and Risk characterization and quantification (DAT)

Detailed hazard characterization of a probable threat during tunnel constructions will be done in coordination with the stakeholders. These will include numerical modeling and probabilistic analysis for hazard function determination.

Development of methodologies and code to perform quantitative risk assessment of large-scale tunneling projects. It includes developing algorithms to assess different construction strategies (construction methods and sequences, mitigation, and remediation measures of interest to the stakeholders) that can be used to refine construction strategies in a real project. This Task adapted and customized DAT (Decision Aids for Tunnels), an existing interactive support system for tunneling construction simulation, to the evaluation of large-scale projects.

TASK 4 – Construction phase: Advance Rate Forecast for TBM

TBM is the prevalent mode of construction that will be used in the construction of the new Hudson tunnel. Predicting Penetration (PR) is crucial to predict Tunneling Boring Machine (TBM) performance and estimate the construction time and cost of a TBM tunnel. In this task we developed a ML based PR forecast model during construction that uses sensor data collected by the TBM as input. To test the models, we used data from an already constructed TBM tunnel in Portugal, as the Hudson tunnel construction has not started yet.

2 Detailed Descriptions of Tasks 1 through 4

In the main body of the report, we summarize what was done in each task, the approach, and the findings.

2.1 Task 1 Geologic and construction data collection

Case study: new Hudson tunnel

To achieve the objectives of the research project and to demonstrate the tools developed we used the newly proposed Hudson tunnel as a case study.

The Hudson Tunnel Project's goal is to preserve the current functionality of Amtrak's NEC service and NJ TRANSIT's commuter rail service between New Jersey and PSNY by repairing the deteriorating North River Tunnel, and to provide redundant capability to those services once the North River tunnel is repaired. The Preferred Alternative of the Hudson Project consists of a two-track passenger rail tunnel on the NEC between New Jersey and New York, referred to as the Hudson River Tunnel, and rehabilitation of the existing North River Tunnel. The preferred alternative alignment is shown in Figure 1.

Figure 1 Hudson Project: Preferred Alternative alignment

The major components of the Hudson Project are:

New Jersey surface alignment. This component consists of surface tracks on embankments and viaducts (blue and red in Figure 1). It begins in Secaucus, NJ cutting through North Bergen until the portal of the new tunnel.

New Hudson River Tunnel. The tunnel (orange in Figure 1), which is a proposed to have two tracks in two separate tubes, consists of three stretches: New tunnel in New Jersey, New tunnel beneath Hudson River and New tunnel in Manhattan. Also, part of this component are the several ventilation shafts and fan plants.

Rehabilitation of the existing North River Tunnel. Once the Hudson Tunnel is completed and in operation, rehabilitation will start.

In this project we focused on the planning of the tunnel stretches under the new Hudson River Tunnel, more particularly the stretch beneath the Hudson River.

Geology

A field research study was conducted to identify in detail the geologic conditions along the planned Hudson tunnel alignment. The data collected was based on geotechnical reports and survey data provided to us by the stakeholders, Gateway Corporation, the environmental impact statement, and technical literature [1] and existing geologic maps Figure 2.

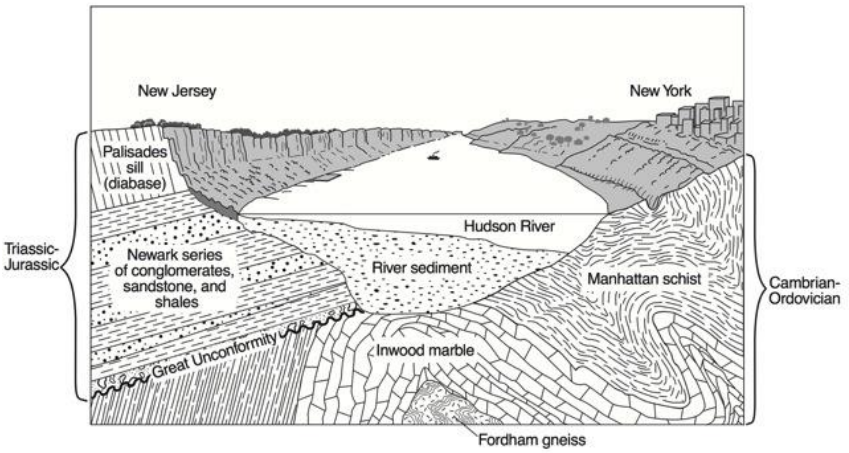

Figure 2 Geological profile at the Washington Bridge site. Image Credit: illustration by Charles P. Berkey, 1948.

The literature reviewed revealed not only the existing geological conditions along the tunnel Hudson alignment but also the main most likely geohazard. Regarding the geological conditions, on the New Jersey side, most of the tunnel will go through the Newark basin, comprised mostly of a sequence of sandstone and shales. Metamorphic rocks in the project area occur only along the Hudson River waterfront in Hoboken and Jersey City. Serpentinite is exposed along the Hudson River waterfront at Castle Point in Hoboken and is believed to extend south into Jersey City. The superficial materials overlaying the bedrock of the Hudson River stretch are about 300ft in

thickness. The stratigraphy of the superficial soils is complex and comprises of glacial, fluvial, lacustrine, and estuarine deposits. Regarding the bedrock, the western part of the Hudson River stretch is sedimentary rocks from the Stockton formation. The Eastern part of the Hudson River stretch is underlain by metamorphic rocks of the Manhattan Prong. Serpentine and Schist are the dominant rock formations. On the Manhattan side, most of the study area is underlain by Schist believed to belong to the Hartland Formation. The superficial geology in New York City consists of glacial till overlain by silt and clay, estuarine and marsh deposits, and silty sand, and its thickness is often less than 50 feet across most of Manhattan. However, in the study area the superficial geology is much thicker since the bedrock near the Hudson River is at a much greater depth. Near the Hudson River (Manhattan side), superficial geology is primarily fill reclaimed from the river.

Hazards

The potential adverse impacts to the construction of the tunnel due to the existing geology pointed out by the Environmental Impact Statement (EIS) were:

1. Potential instability of existing building foundations.
2. Soil erosion and degradation.
3. Tunnel face instability due to tunneling through mixed-face (soil and rock mixture) and unstable bedrock.
4. Potential disturbance of hazardous minerals
5. Slope instability from construction vibrations.
6. Generation of vibrations from blasting
7. Subsidence due to the dewatering

For this project and the demonstration of the tools developed we focused on hazard 3., i.e., tunnel face instability and the potential water inflow due to tunnel face instability.

2.2 Task 2 Stochastic Geologic modeling

Initial geologic profiles were then developed for the Hudson Tunnel. Developing the initial maps for the new Hudson Tunnel involved establishing an important collaboration with the Gateway Corporation. Specifically, Gateway Corp provided crucial subsurface information, including borehole log data and geotechnical reports. The maps developed for Hudson tunnel alignment were based on a field research study conducted in the initial 3-month period of the project that collected, amongst other things, hard copies of borehole log information and subsurface cross-sections.

The hard copies of the subsurface data were digitized and Geographic Information Systems (GIS)-based methods [2] were used to produce 3D models of the area'. Such initial geology location maps require further developments and refinements for producing the final representative maps of the subsurface.

In this task, we developed an ML-based model to predict the lithology of the ground associated to a section of the Hudson Tunnel Project. Data sources for developing the model include 63 excavated boreholes along the proposed tunnel path. The borehole location can be seen in Figure 3.

Figure 3 Borehole location within the research area

The initial geologic maps were developed based on survey data that was provided to us by Gateway Corporation, as described above. The information on the geological maps was used as input to Task 3.

2.2.1 Artificial intelligence framework

2.2.1.1 Random Forest (RF)

Random forest (RF) is a nonparametric tree-based ensemble technique [3,4] which does not contain parametric models, in contrast to conventional statistical methods, but contains numerous easy-to-interpret decision trees [5]. Each tree consists of a decision like structure containing multiple nodes which might include either a conditional statement or a prediction. Integrating the results of the analysis of decision tree models enables the development of a more comprehensive prediction model.

In RF models, each tree selects a small set of features in the single-tree building process. This mechanism allows the RF to run a large-scale attribute set (i.e., a dataset with large number of input variables or features) , at an acceptable time frame. In random forests, a sufficient number of trees should be used to ensure adequate contributions to all participating features. Each random forest classification tree is constructed with a new training set (i.e., a bootstrap sample) replacing the original training set. This classification ensures random selection of drawn training data from the original dataset for construction of each decision tree. The remaining data are not involved in the tree training process, so they are referred to as out of bag (OOB). The OOB subset is later used to evaluate the constructed tree [4,5]. In summary, the RF method contains three main steps: (1) separation of a random sub dataset from the original data, (2) sampling data subset to build a predefined number of trees, and (3) combining the results of trees by selecting the majority classified label.

2.3 Neural Network (NN)

Neuronal networks are composed of many simple elements or nodes called neurons which contain a mathematical function with the purpose of finding the weighted average of its inputs and are arranged into layers. These neurons are connected to each other by many links. These links contain a coefficient which is referred to as weight which represents the importance of origin of the link for its destination. A random value is assigned to each weight at the start of the learning process and during the training phase they are adjusted to acquire the correct output. The input of a neuron is multiplied by the weight of the neuron. Then sums of the products are fed to a transfer function to create the output. This can be expressed in the form of following equation:

$$z = f(\sum_{i=1}^{n} w_i \, x_i + d)$$

where z is the output, x_i is the input, w_i is the weight of the link, d is bias value, and f is the transfer function. The connection weight and bias values are initially selected as random numbers and then determined by the results of the training process.

In each neural network the first layer is the input layer, the last layer is the output layer, and any connecting layer between these two are called hidden layers (Figure 4). In the layered structure of Neural Network, the output of the first layer is the input of the next layer, and it goes on until the last layer that provides output of the model. Given a sufficient number of neurons and hidden layers, any hidden pattern and trends between input and output variables can be detected. The number of neurons in the first layer must be equal to the number of features, and in classification problems, the number of neurons for the last layer must be equal to the number of existing categories in the target variable. Using the SoftMax activation function, a function available in Python, for each neuron leads to a probabilistic output for each category. The SoftMax function provides the probability of each number in a vector. This is done by assuming each probability is equal to the value of that element in the vector divided by sum of all elements in the vector. The goal of the procedure is to maintain generalization of the model while reducing the error in classification.

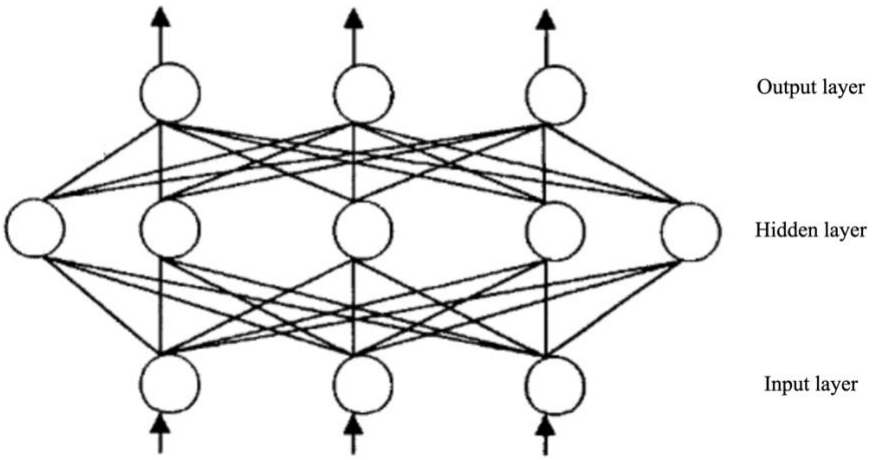

Figure 4 Simple Neural Network structure [6]

2.3.1 Random search hyper-parameter tuning

Each machine learning technique includes multiple predefined hyper-parameters that control their algorithm. Searching for the best combination of hyper-parameters should be a vital part of any machine learning study. However, Finding the best combination of these parameters can be a daunting task. A random search technique uses a predefined number of random combinations of values in the hyper -parameter space to find the combination that develops the most accurate model (Figure 5). It was observed that a large number of trials can lead to significant increase in accuracy of the model. Random Search has been one the most used machine learning tuning techniques since it is based on a simple algorithm and in comparison to other common optimization techniques such as Grid Search, it is much less time consuming without any significant loss in performance [7]. Table 1 shows the hyper-parameter space for Random Forest and Neural Network model. These parameters are in detailed defined in SKLearn [8] and Keras [9] documentations.

The hyper-parameters for the Random Forest model include the number of decision trees in the forest, number of features used to train the model, maximum depth of each tree which is also the number of splits before leaf node, minimum number of splits in each tree, minimum number of leaf (terminal) nodes in each tree which contain the prediction values, and whether the dataset used for training each tree can contain repetitive data points or not.

The hyper-parameters in Neural Network model include how many time the network should be trained (epoch) , the number of data points used in each training trial (Batch size), the learning rate which is the adaptation speed of the model to the problem (large learning rate can converge to a solution faster, however, that solution might be suboptimal), the momentum factor which is the proportion assigned to previous steps' gradient of error, and optimization functions used in each layer.

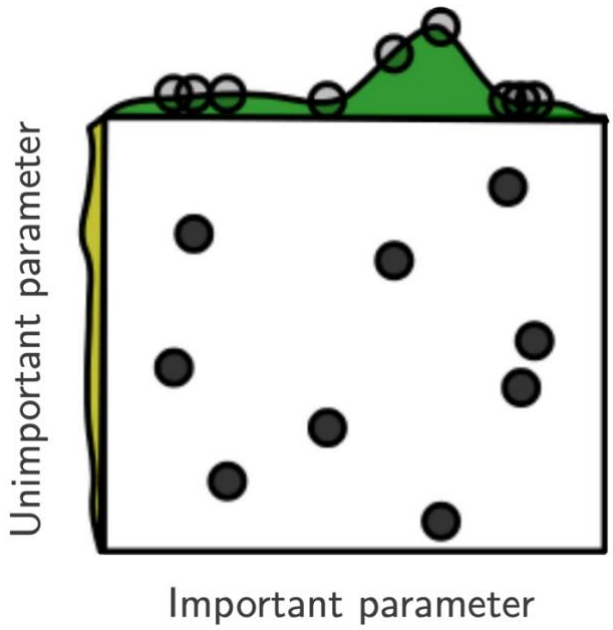

Figure 5 Random search hyperparameter tuning selection of points for two hyperparameter subspaces including one important and one unimportant variable [10]

Table 1 Hyper-parameter space for Random Forest and Neural Network models

Hyper-parameter	Range
Random Forest	
Number of trees in the forest	200, 210, 220, …, 2000
Max number of features in each tree	Auto, sqrt
Max depth of each tree	10, 20, 30, …, 100
Min number of splits in each tree	2,5,10
Min number of terminal nodes in each tree	2, 4, 8
Replacement in data subset selection for each tree	True, False
Neural Network	
Number of training the network (Epoch)	10, 20, 40, 60, 80, 100
Size of batch for training (Batch size)	10, 50, 100
Learning rate	0.001, 0.01, 0.1, 0.2, 0.3
Momentum factor	0.0, 0.2, 0.4, 0.6, 0.8, 0.9

Optimizer function for each layer	'SGD', 'RMSprop', 'Adagrad', 'Adadelta', 'Adam'

- SGD: Stochastic gradient descent, RMSprop: Root mean squared propagation, Adagrad: Adaptive gradients, Adadelta: Adaptive learning rate gradient descent, Adam: Adaptive moment.

2.3.2 Evaluation Metrics

2.3.2.1 Performance metrics

In this study, four different performance metrics including accuracy, precision, recall, and F1 score are used and defined as follows:

$$accuracy = \frac{number\ of\ correct\ categorized\ data\ points}{total\ number\ of\ data\ point}$$

$$precision = \frac{TP}{TP + FP}$$

$$recall = \frac{TP}{TP + FN}$$

$$F1 - scroe = 2 * \frac{precision * recall}{precision + recall}$$

where, TP is true positive, FP is false positive, TN is true negative, and FN is false negative. True positive is when the model correctly predicts category, false positive is the instance that the model falsely predicts a category, true negative is when the model correctly predicts that a category does not occur, and false negative is when a category occurs but the model incorrectly predicts that it doesn't occur. Therefore, recall is the ability of the model to find the dataset in a certain category and precision is the ability of the model only the data points in a certain category. F1 score tries to integrate recall and precision using harmonic mean [11].

2.3.3 Data Collection and Data Structure

The data used in this study was collected from the Hudson tunnel project and specifically the tunnel section aligned under the Hudson River [12]. This section is chosen because of its complex geological structure and interaction with the river. The lithology in this section was divided into five categories fill, clay, sand, rock, and ground improvement. Since the ground improvement is a man-made structure and the geometry and location associated with ground improvement is well established, the ground improvement section is removed from the data. The lithology data was acquired from the 65 boreholes along the tunnel alignment. These wells start at the top surface or bottom of the river and are up to 200 feet deep.

The extracted data from the boreholes was then preprocessed to be fed to the AI models. Along each borehole at equal intervals (i.e., the seed interval), lithology is extracted from the borehole logs. Three-dimensional coordination of that point was then calculated. Therefore, each datapoint includes X, Y, Z coordinates and lithology of the soil at that geometric location. In the testing phase, X, Y, Z coordinates are given to the trained model and lithology is predicted.

2.3.4 Methodology

The proposed models are implemented in the Python language. Figure 6 shows the methodology followed in this study in terms of data input, algorithm implementation, and data output. The first step is to import the borehole log into the programming environment. The extracted data is pre-processed and prepared for AI use by finding geological coordinates of the boreholes and lithology type at different depths of the boreholes and putting this information in a tabular format. The data is then divided into testing and training data depending on the required scheme of the study. Multiple testing and training data sets were considered in this study. Then from each AI model multiple candidate models are developed to find the best hyperparameter for Random Forest and Neural Network Models. The best estimator is then used to predict the testing subset of data and evaluate the model.

Different factors can affect the results of the models including data extraction interval, borehole quantity, boundary conditions on top and bottom of the boreholes, and geological complexity. Multiple scenarios were designed and used to develop models to assess the sensitivity of proposed algorithm to these factors.

The base scenario consists of using one borehole log data as part of the testing data subset and the rest of boreholes data are used for training of the models. The data is extracted from the borehole logs at 1 ft intervals.

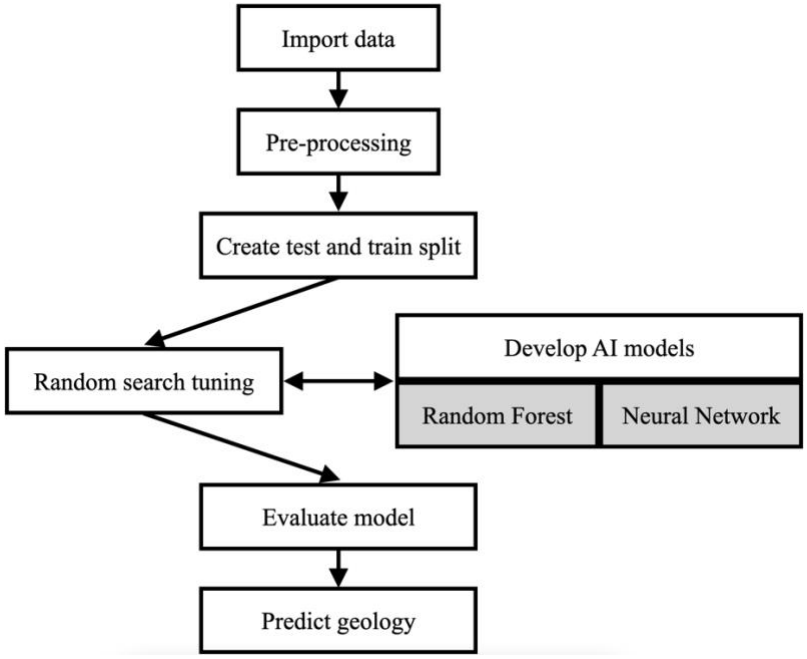

Figure 6 Developing the model Process

2.3.5 Results and Discussion

2.3.5.1 Random Forest

The base case was carried out using the Random Forest technique. Table 2 shows the average performance metrics for all the boreholes. As shown in Table 2, the proposed model has an average 0.86 accuracy which is an excellent accuracy compared to literature which is around 0.8 [13]. Precision, Recall, and F1_score is 0.74, 0.75, 0.72 which also at an acceptable range [14].

Table 2 Performance metrics of Random Forest model for base scenario

Model	Accuracy	Precision	Recall	F1_score
Random Forest	0.86	0.74	0.75	0.72

Furthermore, Figure 7 shows a comparison of the observed soil profile in PE-225 borehole and the predicted soil profile by the proposed model as an example. As can be seen, the model provides excellent accuracy in prediction of the soil profile. Appendix A shows comparison of soil profile for all the boreholes predicted by Random Forest model. Figure 8 Shows accuracy of Random Forest for each borehole separately.

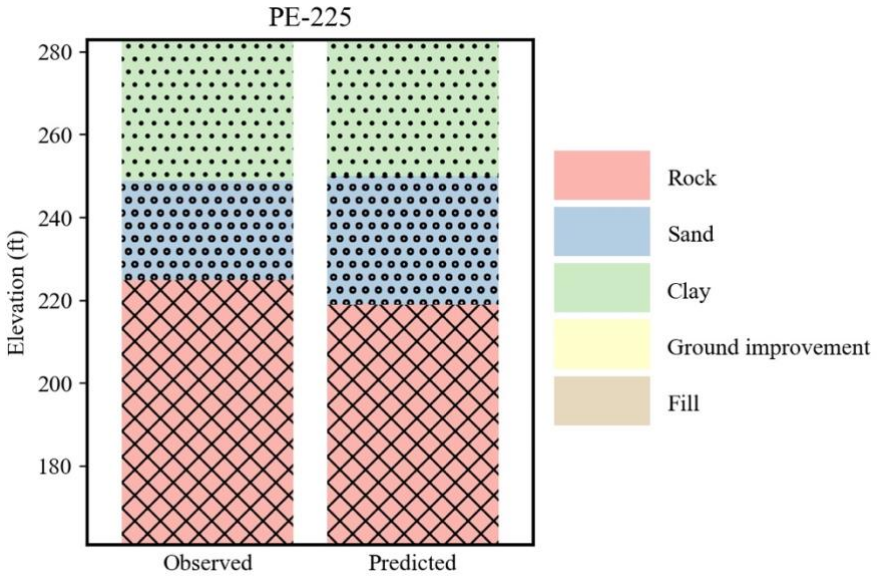

Figure 7 Predicted soil profile versus observed soil profile at one borehole by Random Forest model

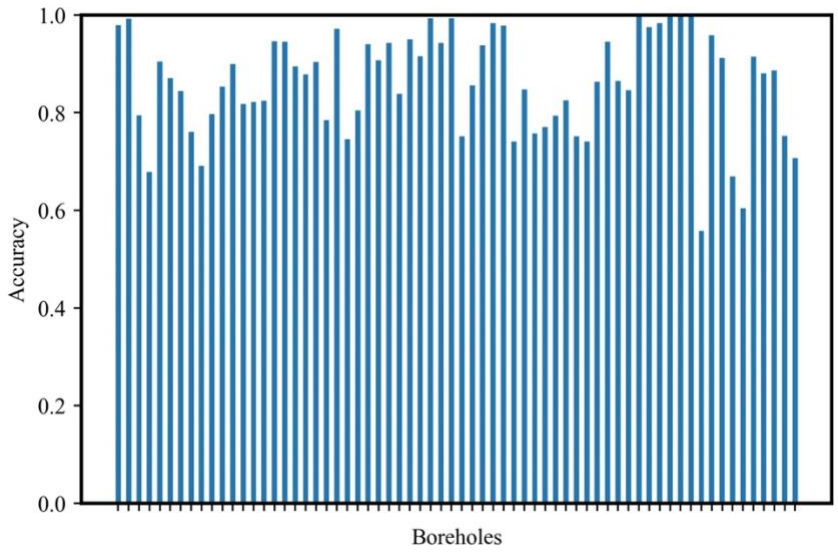

Figure 8 Accuracy of Random Forest model for each borehole

2.3.5.2 Neural Network

Table 3 provides average values for all borehole performance metrics for the Neural Network model. The accuracy of the model is 0.81 which is 6 percent less in comparison to the random forest model for the same simulation. Precision, Recall, and F1_scores were 0.65, 0.66, and 0.62 respectively. The fact that they are much lower than accuracy shows an imbalance in prediction of some categories. This is due to the fact that these values, at each borehole, are calculated by averaging precision, recall, and F1-score for each category. Therefore, large difference between accuracy and other metrics shows an imbalance in prediction of the model prediction. In other words, Neural Network predicts some categories with much higher accuracy than others.

Table 3 Performance metrics of the Neural Network model for the base scenario

Model	Accuracy	Precision	Recall	F1_score
Neural Network	0.81	0.65	0.66	0.62

Figure 9 Shows the prediction versus observe of soil profile at borehole PE-225. In comparison to Figure 7, it can be seen that the Neural Network model is less accurate than Random Forest. Appendix B shows the prediction of the borehole profile for the rest of the boreholes. Figure 10 Illustrates accuracy of Neural Network model for all boreholes.

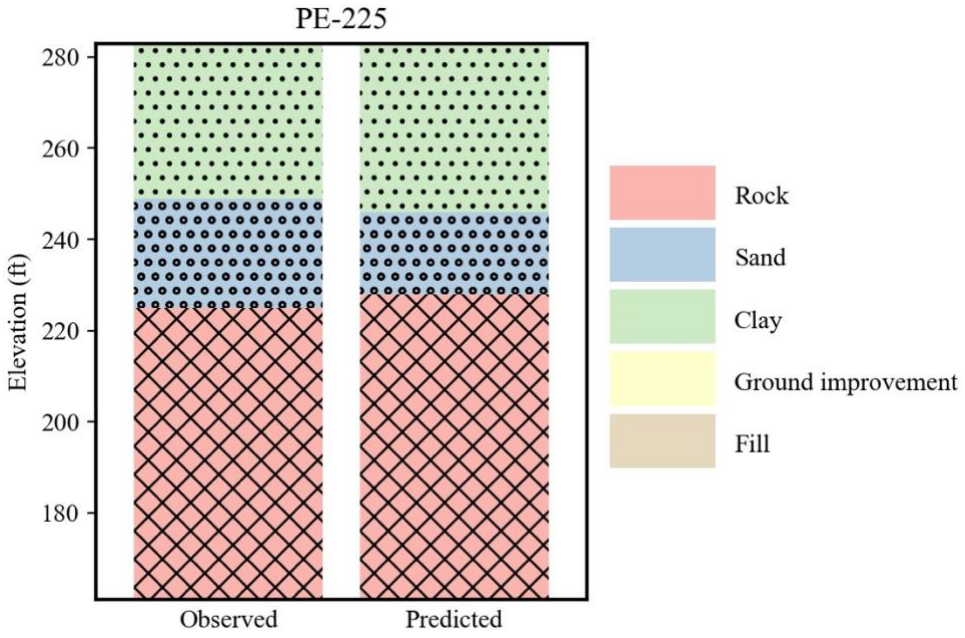

Figure 9 Predicted soil profile versus observed soil profile in one borehole using the Neural Network model

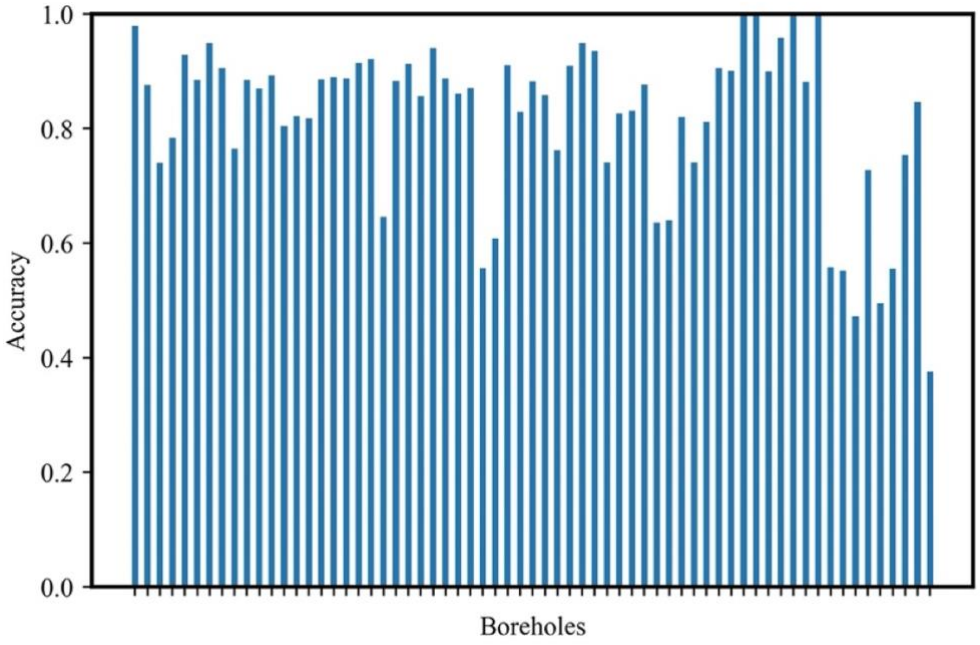

Figure 10 Accuracy of Neural Network model for each borehole

2.3.5.3 Data extraction distance effect

Different vertical distance of data extraction was used to investigate the sensitivity of the models to vertical positioning. Two different data extraction distances were used: 1 ft and 0.5 ft. Table 4

shows the performance of Random Forest and Neural Network with each of these distances. As can be seen, the Neural Network accuracy increased by 2.5% to 0.83 by decreasing the extraction distance from 1 ft to 0.5 ft. However, the overall accuracy of the Random Forest was unchanged at 0.86. The same trend was seen in other performance metrics.

Table 4 Effect of data extraction distance on performance of the models

Model	Accuracy	Precision	Recall	F1_score
1 ft intervals				
Random Forest	0.86	0.74	0.75	0.72
Neural Network	0.81	0.65	0.66	0.62
0.5 ft intervals				
Random Forest	0.86	0.75	0.75	0.72
Neural Network	0.83	0.69	0.66	0.65

2.3.5.4 Borehole Quantity Influence

Another factor that can affect the accuracy of the model is the number of borehole logs used to train the model. In order to study this factor, each model was trained with data from n number of boreholes which are closest distance to the testing borehole. Table 5 contains performance metrics for models trained with 3, 5, 7, and 9 closest borehole data and the base scenario. For Random Forest model using 3 borehole data leads to highest accuracy, however, the difference in accuracy is negligible. For Neural Network the highest accuracy belongs to the base model, and again this is only slightly better than other cases. This shows that sensitivity of both models to the number of boreholes data are negligible, and they are mostly dependent on the closest borehole data.

Table 5 Effect of number of borehole data used for training the model on performance of the model

NO. Boreholes	Accuracy	Precision	Recall	F1_score
Random Forest				
3	0.87	0.78	0.77	0.75
5	0.86	0.76	0.75	0.73
7	0.86	0.76	0.75	0.73
9	0.86	0.76	0.74	0.72
Base case	0.86	0.74	0.75	0.72
Neural Network				
3	0.80	0.63	0.64	0.6
5	0.78	0.60	0.63	0.58
7	0.80	0.60	0.64	0.59
9	0.80	0.62	0.63	0.60
Base case	0.81	0.65	0.66	0.62

2.3.5.5 Boundary Effect

One of the factors that can affect the accuracy of the model is geology condition at the two ends of the boreholes. The models are more prone to mistakes due to discontinuation of data at these

locations. Further, the depth of a borehole varies based on positioning and geological profile, causing additional boundary effects. To remove the influence of these factors, data points were restricted to the middle 60% of the length of each borehole (Figure 11). Since the tunnel passes through the middle part of the boreholes, this accuracy is also more practical for the tunneling problem.

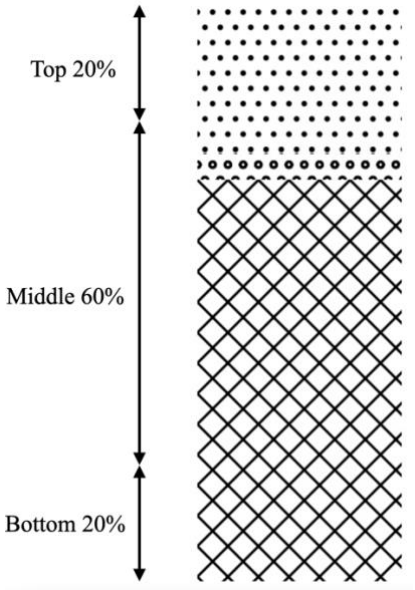

Figure 11 Division of each borehole log for boundary effect analysis

Table 6 contains the performance of the model in the middle 60% section of each borehole and 100% of data from each borehole. To perform this analysis, one borehole was selected as testing borehole and the rest was used as training boreholes. After training the model, the average performance metrics at points along the borehole were calculated. Next, the average metrics in the 60% middle sections points were assessed. It can be seen that the performance of Random Forest model is less sensitive to the boundary structure, and it shows the same accuracy in both cases. However, for the Neural Network, considering only the middle section of each borehole increased the accuracy to 0.83 from 0.81. This is an indicator of the sensitivity of the Neural Network to the boundary conditions of the geology.

Table 6 Performance of the models with and without borehole tips

Borehole section	Accuracy	Precision	Recall	F1_score
Random Forest				
All sections	0.86	0.74	0.75	0.72
Middle section	0.86	0.70	0.72	0.68
Neural Network				
All sections	0.81	0.65	0.66	0.62
Middle section	0.83	0.64	0.66	0.63

2.3.5.6 Geological Complexity and Borehole Density

The geology of the Hudson River case study can be divided into three main categories, shore, under the river, and transitional (Figure 12). The first two categories consist of simpler geology with less sudden movement of interface in their zones, however, during the transition from shore to under the river, the geology experiences complicated and sudden changes. However, the density of the boreholes in Sections 1 and 2 were much higher than other sections.

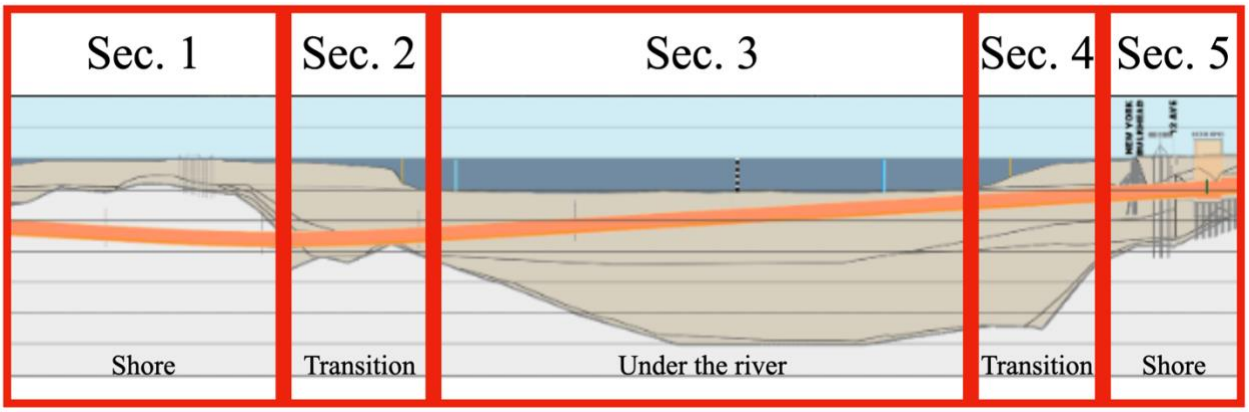

Figure 12 Division of the tunnel to various sections for geological complexity and borehole density analysis [15]

To ensure acceptable performance of the models during these transitions, tunnels were divided into 5 sections, and the average performance of the model at each section is provided in Table 7. The Random Forest model in sections 1, 2, and 3 has an accuracy of 0.84. However, in sections 4 and 5 the accuracy drops to 0.78 and 0.79 respectively. The same trend can be seen in the performance of the Neural Network model. However, the average accuracy of the model falls more sharply to 0.56, 0.61 for Sections 4 and 5, respectively. The results show that both models are more sensitive to the density of the wells than to the complexity of the geology. In other words, with a high number of boreholes, the proposed models can overcome the complexity of the geology and show high accuracy in prediction of geological profile.

Table 7 Performance of the models developed in different sections of the tunnels

Tunnel Section	Accuracy	Precision	Recall	F1_score
Random Forest				
Section 1	0.84	0.67	0.70	0.65
Section 2	0.84	0.67	0.70	0.65
Section 3	0.84	0.65	0.67	0.63
Section 4	0.78	0.64	0.64	0.62
Section 5	0.79	0.62	0.60	0.57
Neural Network				
Section 1	0.85	0.70	0.68	0.66
Section 2	0.82	0.68	0.72	0.66
Section 3	0.93	0.75	0.72	0.72
Section 4	0.56	0.23	0.30	0.26
Section 5	0.61	0.42	0.48	0.42

2.4 Task 3 Geohazard, Risk characterization, and quantification

Decision support systems for the planning of robust high-speed rail systems considering the effects of natural hazards exist [16] and have been applied to real transportation problems [16]. These systems were reviewed to determine the requirements for incorporating the geohazards in the context of the transportation systems planned for the New York / New Jersey area.

To achieve the objectives of this project, we customized an existing decision support system – the decision aids for tunneling (DAT) – to analyze the hazards and risks of the Hudson Tunnel's construction. Applying such a decision support system entails the definition of possible scenarios representing potential geohazard and the impacts on built transport infrastructure. The new Hudson Tunnel faces potential geohazards that must be considered during its design and construction phases. There are several geohazards related mainly to geology, groundwater, and construction methods. To test our tool, we chose to focus on seepage and flooding within the tunnel during its construction which could affect its structural integrity, and we considered two scenarios: 1. Nuisance flooding (no loss of stability) and 2. Catastrophic flooding (loss of stability)

The decision support system then assesses the impact of these hazards on tunnel infrastructure based and its vulnerability to these specific hazards. In practice, the interactive tool can define various scenarios and combine multiple hazards to assess risk and attain a robust infrastructure.

2.5 Task 3.1 Customization of DAT for the Hudson Tunnel and risk quantification

To evaluate the performance of the customized tunnel construction, our study focuses on a specific section of the tunnel that runs beneath the Hudson River, referred to as the Hudson River Tunnel henceforth. This stretch spans approximately 7228 ft, commencing from the Hoboken Shaft and extending under the Hudson River to the 12th Avenue Shaft (referred to as NY Shaft hereinafter) using a tunnel boring machine (TBM). Note that the shafts were also modeled. The research area is illustrated in Figure 13.

Figure 13 Research area

In this area, the TBM excavation encounters a combination of rock and soil, making the excavation process more susceptible to risks, particularly due to potential water inflow. To accurately estimate the cost and time associated with tunnel construction while considering the uncertainties associated with the geology and construction, we employ Decision Aids for Tunnelling (DAT) [17]. DAT is a tool that facilitates the simulation of tunnel construction, enabling the determination of

construction cost and time by incorporating uncertainties related to geology and construction. It comprises four modules: the geology module – which simulates geologies while considering uncertainties related to ground conditions – the construction module – which simulates construction through the geology profiles generated by the geology module – while considering uncertainties related to costs and times of construction – the resource management module – computes and manages resources from crew to materials, and updating module – which is used to update risk predictions during contrition. In this work, we do not utilize the update module as the Hudson tunnel was in its planning phase.

2.5.1 Data processing and geologic profile

One of the crucial inputs for DAT is geology and the associated uncertainties. To generate the geological conditions required for inputting into DAT, we utilized a combination of borehole data, as depicted in Figure 13, and the findings from Tasks 1 and 2. The soil composition along the tunnel's planned route primarily includes fill, clay, silt, peat, sand, and gravel. To simplify the input process, we grouped soils with similar properties together, such as clay, silt, and peat.

Regarding the rocks, we classified them based on their Rock Quality Index (RQD), as this index serves as an excellent indicator of the degree of fracturing within the bedrock. It provides insights into the rock quality and the ease of constructing through this material, which directly correlates with the construction costs. Specifically, the rocks were divided into two groups: one group with RQD values less than 50 and the other group with RQD values greater than 50.

Additionally, within a 1200 ft stretch, the cover is relatively low, typically measuring less than 22 ft. In this stretch, ground improvement techniques were implemented to ensure safe excavation practices. Figure 14 shows one of the longitudinal geological profiles to be input in DAT.

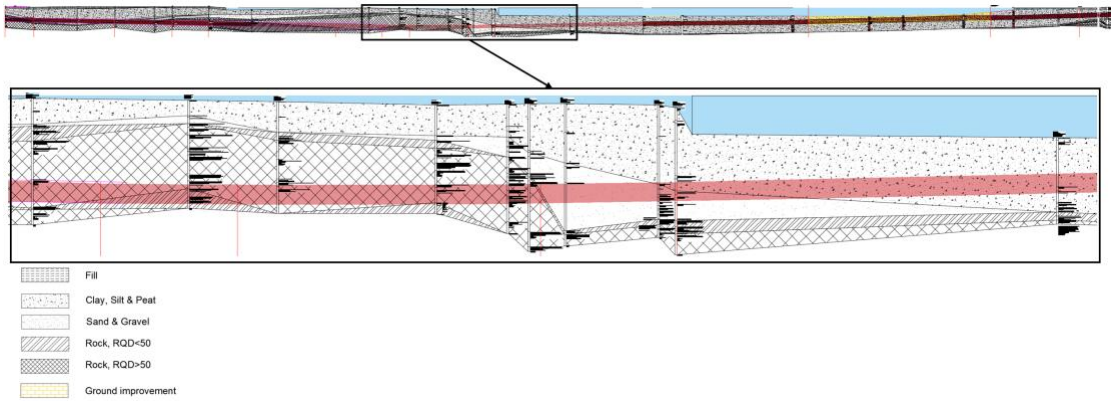

Figure 14 geology conditions of the Hudson River Tunnel

2.5.2 DAT geology input

To incorporate geology into DAT and account for uncertainties, such as variations in geology along the tunnel profiles where precise boundaries between different geologies may not be known, further data processing is necessary. This involves the definition of areas and zones along the tunnel alignment.

These areas and zones are user-defined and typically correspond to sections with similar construction methods or geologies. An area represents a collection of continuous and sequential zones, which can consist of a single zone or multiple zones. The term "zone" refers to a geologically homogeneous unit, essentially a segment of ground where specific parameters and parameter states are expected to occur.

By defining these areas and zones, the geological variations and uncertainties along the tunnel alignment can be systematically incorporated into the analysis within DAT. This enables a more comprehensive assessment of the construction process, considering different geological conditions that may be encountered within each zone.

The division of the tunnel into specific areas and zones for this project is illustrated in Figure 15 Considering the distinct construction processes involved in the Hudson tunnel and shafts, the project was categorized into three main areas: Hoboken Shaft (Area 1), Hudson River Tunnel (Area 2), and NY Shaft (Area 3). Each area represents a distinct segment with unique geological characteristics and construction sequences.

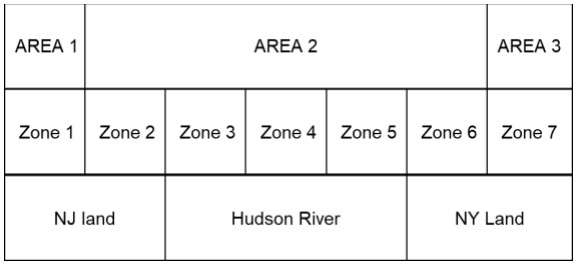

Figure 15 Areas and Zones of the Hudson Tunnel (DAT input)

DAT employs the concepts of Ground Parameters (GPs) and Ground Classes (GCs) to effectively characterize and analyze various aspects of the ground conditions encountered in tunneling projects. GPs are specific parameters related to the ground, such as lithology, Rock Quality Index (RQD), cover condition, groundwater. These parameters provide critical information about the geological characteristics and behavior of the ground. Based on the values and states of these GPs, GCs are defined to represent different combinations of ground conditions. GCs serve to classify and categorize the geological characteristics within specific zones or areas of the tunnel alignment. Each GC is associated with a set of predefined ground conditions that determine the suitability of a particular construction method. By utilizing GPs and GCs, DAT enables a systematic approach to assess and manage the uncertainties and risks associated with different ground conditions in tunneling projects.

In our work, we defined GPs as GP defined in this case are lithology, RQD, cover condition (whether is under river), cover depth, and ground improvement. To initially test the tool, we adopted a deterministic definition of GPs, where each GP was assigned a specific value or state based on available data. However, it is important to acknowledge the uncertainties associated with subsurface conditions, as our knowledge about the ground may be limited. To account for these uncertainties, a probabilistic definition of GPs can be employed. This probabilistic approach

allows for the inclusion of variations and uncertainties in the ground conditions, reflecting the lack of complete knowledge about the subsurface. Figure 16shows the GCs used in this study.

Lithology	Soil			Rock		Soil & Rock
RQD	N/A			>50% & <50%	>50%	>50 % & N/A
Cover	>22'	<22'	>22'	>22'		>22'
Ground improvement	-	Deep soil mixing	Ground Freezing	-		-
GC	1	5	6	2	4	3

Figure 16 Ground classes used in the Hudson Tunnel study.

Instead of utilizing a probabilistic definition of Ground Parameters (GPs) and Ground Classes (GCs), our approach focused on introducing probabilistic variations in the zone limits. In the context of geology zones, there exist uncertainties regarding the precise boundaries of each zone. By making use of the DAT, these variabilities can be incorporated by using a probabilistic definition of the Zones. For this study we used zone lengths that vary by a constant percentage of 10% of each zone's length to consider uncertainties associated with ground conditions [18]. The values of the End Positions (E.P.) of each zone are shown in Table 8. It is important to note that the end positions (E.P.) of each area were maintained as fixed values since the total length of an area is deterministic. By introducing these probabilistic variations in the zone limits, we were able to better capture the uncertainties and variations in the geology, enabling a more comprehensive analysis within the DAT framework.

Table 8 Zones definition in the DAT using probabilistic and deterministic E.P. definitions

Area	Zone number	Zone name	Estimated zone length	Min E.P.	Mean E.P.	Max E.P.
Hoboken Shaft	1	Hoboken shaft	99	99	99	99
Hudson River Tunnel	2	Hoboken land	1320	1188	1320	1452
Hudson River Tunnel	3	Hudson River 1	3852	4787	5172	5557
Hudson River Tunnel	4	Hudson River 2	1200	6252	6372	6492
Hudson River Tunnel	5	Hudson River 3	590	6903	6962	7021
Hudson River Tunnel	6	NY land	266	7228	7228	7228
NY shaft	7	NY shaft	63	63	63	63

2.5.3 Resource management

In addition to modelling geology and ground conditions, it is possible to model resource and resource management with DAT. These resources may include construction materials, excavation materials, labor, and equipment. Their availability, along with the availability of storage space, can significantly impact the construction process and subsequent simulations.

However, in this study, due to limited project information, only one specific resource material, namely muck (i.e., excavation material), is considered. The management and utilization of muck during the tunneling process are analyzed within the DAT framework.

Repositories are established within the DAT model to represent the storage locations from which the tunneling project draws resources or deposits excavated materials. Given that the Hudson River Tunnel is a one-way excavation, two repositories were created: one for Hoboken Shaft and the Hudson River Tunnel, and the other for NY Shaft. These repositories effectively manage the movement of resources and muck throughout the construction process, optimizing resource utilization and logistical operations.

This incorporation of resource materials and repositories within the DAT model adds another layer of complexity and realism to the simulations, allowing for a more comprehensive analysis of the construction process and its associated impacts.

2.5.4 Tunnel construction

The construction of the tunnel was simulated using the construction simulator in DAT. The first step involves defining the *Tunnel Network*. The tunnel Network refers to the interconnected system of tunnels and associated infrastructure that is being analyzed and simulated within the model. It encompasses the various components and paths of the tunnel project, including shafts, cross-passages, branches, and connections. Figure 17 shows the simplified representation of the tunnel network used in this project. However, it is important to note that both Hoboken Shaft and NY Shaft consist of only one path. Due to limitations in presenting a 3D schematic, the tunnel network is split into two paths here for clarity. However, it is essential to emphasize that the construction time and cost are equivalent to a single path excavation.

The construction sequence begins with the completion of Hoboken Shaft. Following a delay of approximately 2 months, the first Tunnel Boring Machine (TBM) starts the excavation of the first tunnel from Hoboken towards NYC, followed by the second TBM which will excavate the second parallel tunnel. The Hudson River Tunnel is excavated from the Hoboken Shaft to the NY Shaft.

Besides the tunnel network, we needed to define the geometric parameters of the tunnels and shafts, which are listed in Table 9.

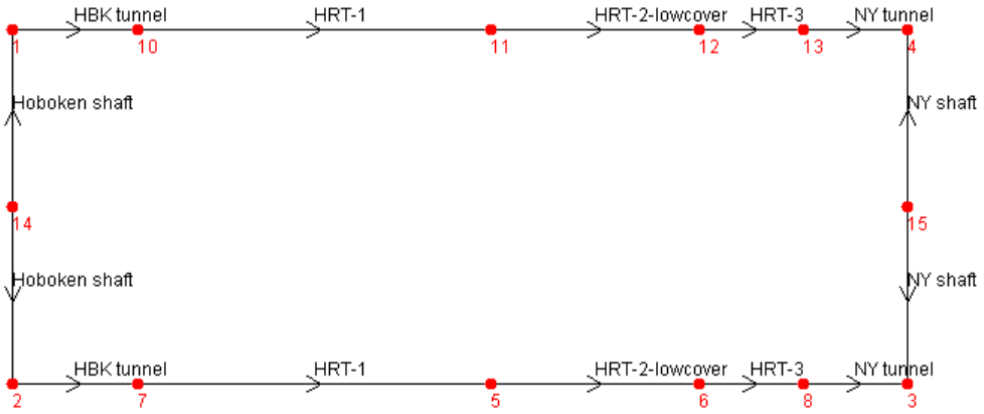

Figure 17 Tunnel network

Table 9 Geometry parameters of tunnel and shaft

Tunnel Outside Diameter	Tunnel Internal Diameter	Tunnel Area	Shaft Diameter	Shaft Area
28 ft	25.16 ft	6158 ft^2	130 ft	13273.2 ft^2

Given the diverse geological conditions encountered in the project, two different excavation methods were planned and thus modelled in DAT: tunnel boring machine (TBM) for tunnelling and drill and blast for shaft excavation. In the modeling process, the construction time and cost were calculated using specific equations.

The construction time and cost were calculated using equations (1) and (2) respectively.

$$\text{Total Time} = t_{mc} + l_r * \text{PCT}_c / (v * f_1 * f_2) \quad (1)$$

where t_{mc} is the delay caused by excavation method change, l_r gives the length of each excavation round, PCT_c returns the percentage of length done during the cycle, v is TBM advance rate, f_1 is efficiency of the crew for the current tunnel, f_2 is efficiency of the crew for the current method.

$$\text{Total Cost} = C_{mc} + C * l_r * \text{PCT}_c \quad (2)$$

where C_{mc} is the additional cost caused by excavation method change, C is the cost per unit length.

The total time for construction, as given by equation (1), is determined by the sum of the delay caused by the excavation method change (tmc) and the time required for each excavation round. The length of each excavation round (lr) is multiplied by the percentage of length completed during the cycle (PCTc), divided by the TBM advance rate (v) and multiplied by the efficiency factors of the crew for the current tunnel (f1) and the current method (f2).

Similarly, the total cost of construction, as defined by equation (2), includes the additional cost caused by the excavation method change (C_{mc}) and the cost per unit length (C) multiplied by the product of the length of each excavation round (lr) and the percentage of length completed during the cycle (PCTc).

It is important to acknowledge that there are inherent uncertainties in both cost and time estimates due to potential changes in the geological conditions. To account for these uncertainties, a range of values is considered for each category, as presented in Table 10. It should be noted that the extreme values in the range are associated with a lower probability of occurrence, as most data points cluster around the central value, with only a few isolated points occurring at the extremes.

Table 10 Cost and time for different categories

	Construction methods	Zones	Min	Mode	Max	Unit
Advance Rate	CDB	Zone 1 and Zone 7	6	13	19	ft/day
	TBM	Zone 2 to Zone 6	25	35	45	ft/day
Cost	CDB	Zone 1 and Zone 7	50	60	70	k$/ft
	TBM	Zone 2 to Zone 6	26	31	36	k$/ft

Note: mode value is the most frequently occurring value of the variable, CDB is drill and blast, and TBM is tunnel boring machine excavation method.

By incorporating these equations and considering the uncertainties in cost and time, the construction simulation in DAT provides a comprehensive analysis of the expected construction duration and cost, considering the variations in geological conditions and excavation methods.

2.5.5 Risk Events

In DAT, risk events associated with the possibility of water inflow during tunnel excavation were defined to assess their impact on construction cost and time. Two types of water inflow risk events were considered: *nuisance flooding* (small water events) and *catastrophic flooding* (severe water inflow with tunnel instability). We considered that these risks events were more likely to occur in the stretch of the tunnel with a cover smaller than 22ft (Zone 4)

Nuisance flooding refers to small water inflow events that can occur during tunnel excavation. These events result in a relatively lower volume of water flow into the tunnel, excavation can progress but still require attention and measures to manage the water. The impact of nuisance flooding includes increased construction cost and a decreased advance rate. To simulate these events in DAT, the cost of construction is doubled, and the advance rate is reduced by half.

On the other hand, catastrophic flooding represents a severe water inflow event with a higher volume of water flowing into the tunnel. This type of flooding can lead to face instability and pose significant risks to the construction process. In DAT, catastrophic flooding events are simulated by triggering the *method change* in DAT. In this case the construction of the tunnel will be interrupted causing delays and remedial work will be done to address the excessive water inflow and possibility associated face collapse. This *method change* leads to delays in construction and additional costs. Table 11 shows how the two flooding events were modelled in DAT. Additionally, we considered a situation where both situations could occur simultaneously.

By considering both nuisance flooding and catastrophic flooding events, DAT enables the assessment of their respective impacts on construction time, cost, and the need for remedial actions. This allows for a more comprehensive understanding of the risks associated with water inflow during tunnel excavation and aids in effective decision-making to mitigate these risks.

Table 11 Water inflow treatment methods description

Risk Event	Defined in DAT by	Description
Catastrophic Flooding	Method change	Every time tunnel encounter large water inflow, delay and additional cost are generated. Using this method, total delay and additional cost induced by water inflow would be related to number of occurrences.
Nuisance Flooding	Increase cost but decrease advance rate	Where small water inflows occur, the cost is doubled, while advance rate is reduced to half.
Both	Combination	In addition to the delay and cost added due to large water inflow, cost is doubled, and advance rate is reduced to half.

As before, the construction time and cost associated with water inflow treatment is uncertain due to the variability of inflow volume. The definition of the associated triangular probability distributions of the delay and additional costs are shown in Table 12. Table 13 shows the triangular probability distributions of advance rate and cost associated with nuisance flooding (or small water inflow)

Table 12 Delay and additional cost for method change to simulate the consequences of a catastrophic flood event (triangular probability distribution)

	Min	Mode	Max
Delay (day)	5	5	10
Additional cost (k$)	250	340	460

Table 13 Advance rate and unit cost associated with small water inflow (triangular probability distribution)

	Min	Mode	Max
Advance rate (ft/day)	12.5	17.5	22.5
Unit cost (k$)	26.36	31.36	36.36

Water inflow event is simulated in DAT using a Markov process. To perform this simulation, two parameters need to be defined: the proportion of no inflow to inflow and the number of occurrences. In this study, the proportion is set to 0.9 (representing no inflow) and 0.1 (representing inflow). The number of occurrences is set to 5.

By incorporating these parameters, DAT can calculate the mode length of the affected areas. The mode length represents the most common or frequent length of the areas affected by water inflow. This calculation is performed using the equation below:

$$Mode\ length = \frac{Total\ zone\ length}{Number\ of\ occurrences} \times proportion \quad (3)$$

In this study, four scenarios were simulated to compare the effects of water inflow on tunnel construction. These scenarios include:

No water inflow (no risk events – only geology and construction uncertainties)

Catastrophic Flooding (possibility of occurrence of large water inflows in the low cover stretch)

Nuisance Flooding (possibility of small water inflows in the low cover stretch)

Both Nuisance and Catastrophic Flooding (possibility of occurrence of both large and small water inflows)

The simulations were conducted using 100 geology simulations and 100 construction simulations. Each simulation considered the probability distributions of zone length, advance rate, and cost for each construction strategy, as well as the delays and additional costs caused by water inflow. This resulted in a total of 10,000 simulations.

2.5.6 Results

The cost-time scattergram, shown in Figure 18, illustrates the relationship between construction cost and time for each scenario. The frequency distributions of the simulations are fitted to a Gaussian distribution.

It is noteworthy that simulations without water inflow exhibit less variability in both time and cost compared to the other three scenarios (where flooding was considered). This is because the absence of water inflow eliminates delays and additional costs. Conversely, simulations with large water inflow exhibit greater variability in time, while simulations with small water inflow exhibit greater variability in cost. The combined methods scenario demonstrates increased variability in both cost and time, as expected. The presence of water inflow not only introduces variability to the results but also incurs additional time and cost during tunnel construction. The specific changes in delay and additional cost caused by water inflow are summarized in Table 14.

These findings highlight the importance of considering water inflow in tunnel construction planning and the potential impact it can have on project timelines and budgets.

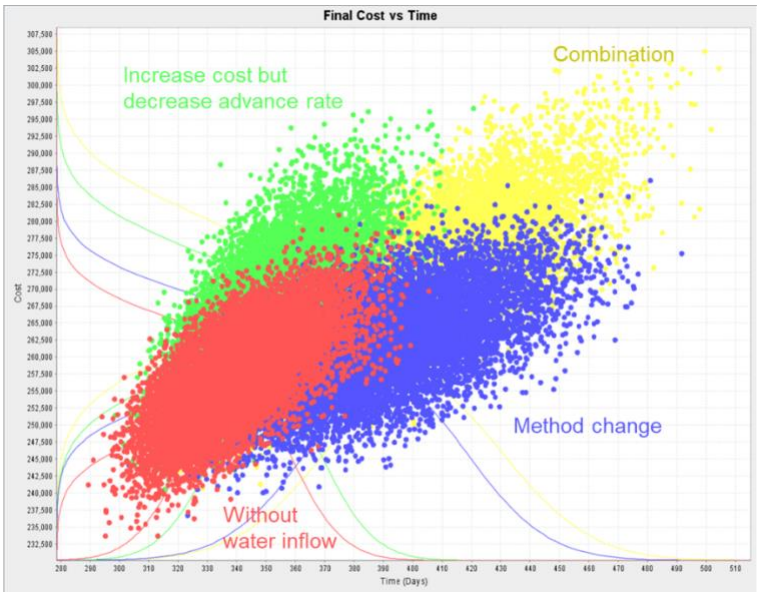

Figure 18 Cost-time scattergram results of different flooding scenarios

Table 14 Delay and Additional Cost induced by water inflow

Method	Mode delay (day)	Mode additional cost (k$)	Method
Method change	40	1700	Large water inflow
Increase cost but decrease advance rate	3.4	3736.2	Small water inflow
Combined	43.4	5436.2	Combination

DAT also provides the capability to output specific cost and time information for each zone, allowing for a detailed understanding of the excavation process. Figure 19 and Figure 20 demonstrate how DAT can present the cost and time distribution along the tunnel alignment. This visualization enables a comprehensive view of the progress and resource utilization at different positions within the tunnel.

Furthermore, DAT also allows for monitoring repository stock information (Figure 21). This feature enables the tracking of resources, such as construction materials or excavation materials, stored in the repositories. By monitoring the repository stock, project managers can ensure an efficient supply of resources throughout the construction process.

This feature of DAT provides valuable insights into the excavation process by offering detailed cost and time information for each zone and facilitating the monitoring of repository stock information.

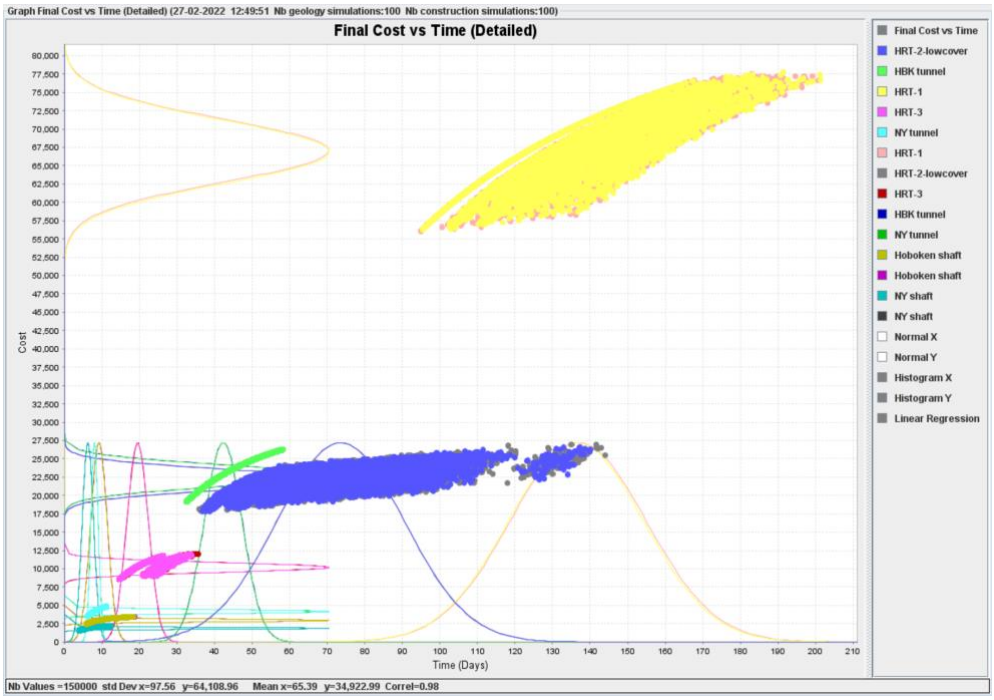

Figure 19 ailed cost and time for different zones of the Hudson tunnel

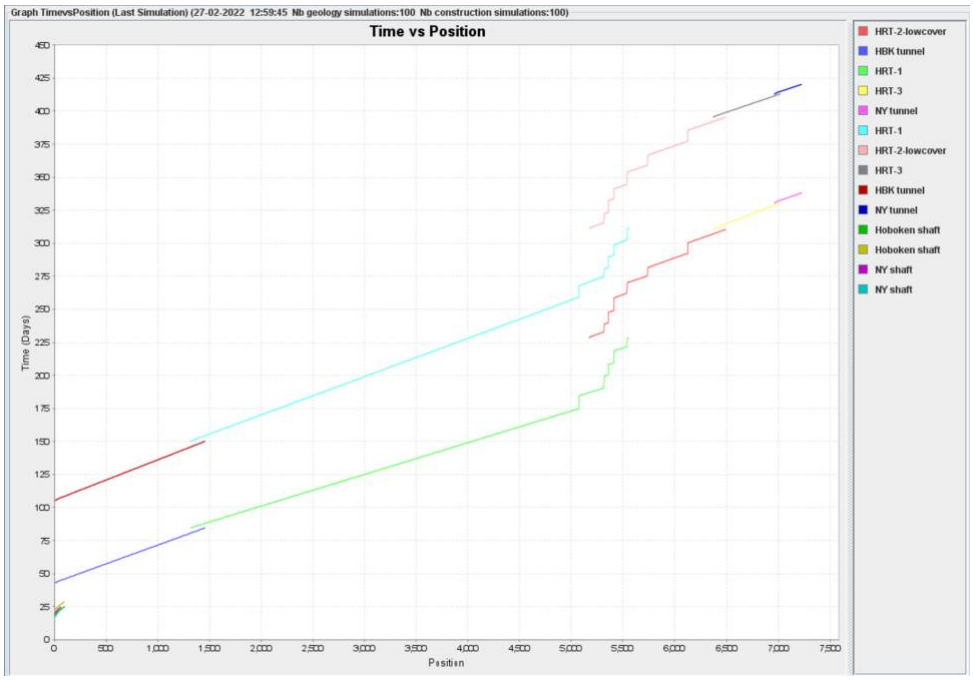

Figure 20 Time vs Position (Hudson Tunnel)

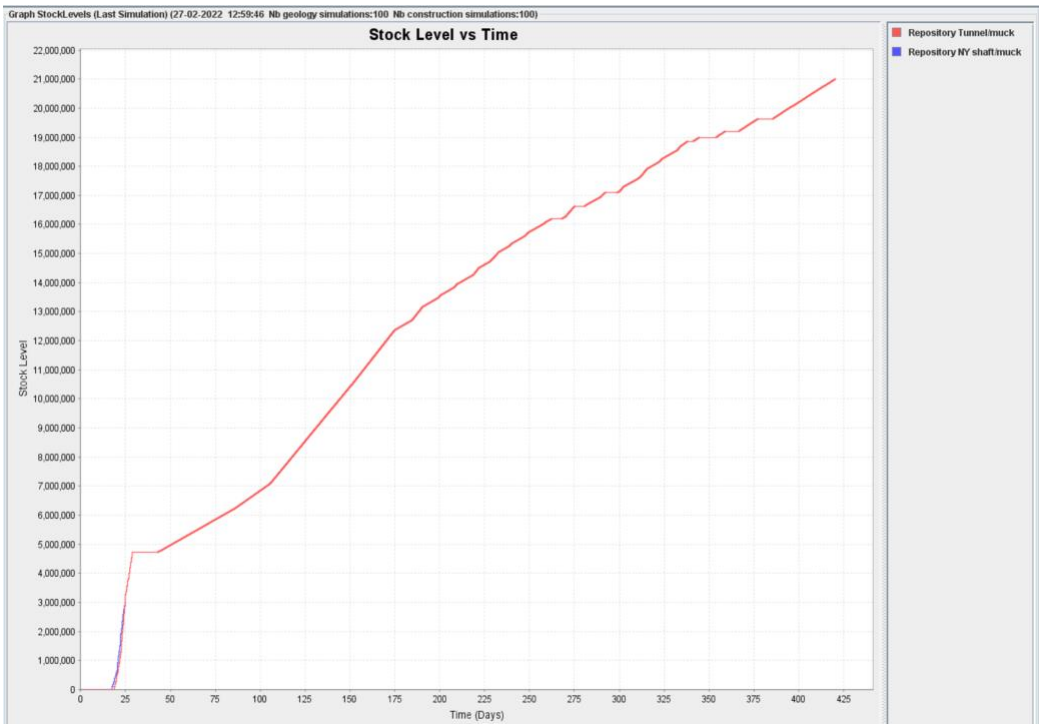

Figure 21 Stock vs Position (Hudson Tunnel)

2.5.7 Sensitivity analyses

We conducted sensitivity analyses to assess the influence of key parameters on the risk assessment of tunnel construction, specifically the time and cost implications. The parameters under investigation included the number of occurrences of water inflow, the proportion of no inflow to inflow, the additional cost and delay associated with large water inflow, and the cost and time changes associated with small water inflow. For this analysis, we focused on the scenarios involving large and small water inflows, omitting other scenarios to maintain simplicity. This analysis allowed us to identify which parameters had the most significant influence on the time and cost of tunnel construction, providing valuable information for decision-making and risk mitigation strategies.

2.5.7.1 Number of occurrences

Firstly, we conducted a sensitivity analysis on the number of water inflow occurrences. It should be noted that this analysis only pertains to the scenario of large water inflow, and small water inflow is not considered in this analysis. The cost-time scattergram in Figure 22 illustrates the results of this sensitivity analysis. In the analysis, we examined three different values for the number of occurrences: 5, 25, and 50. The scattergram demonstrates that a higher number of occurrences corresponds to increased delay and cost and a wider spread of the scatter cloud. This observation can be attributed to the positive relationship between delay, additional cost, and the

number of occurrences. When the number of occurrences is high, the uncertainty in additional cost and delay increases, leading to more significant outcome variability.

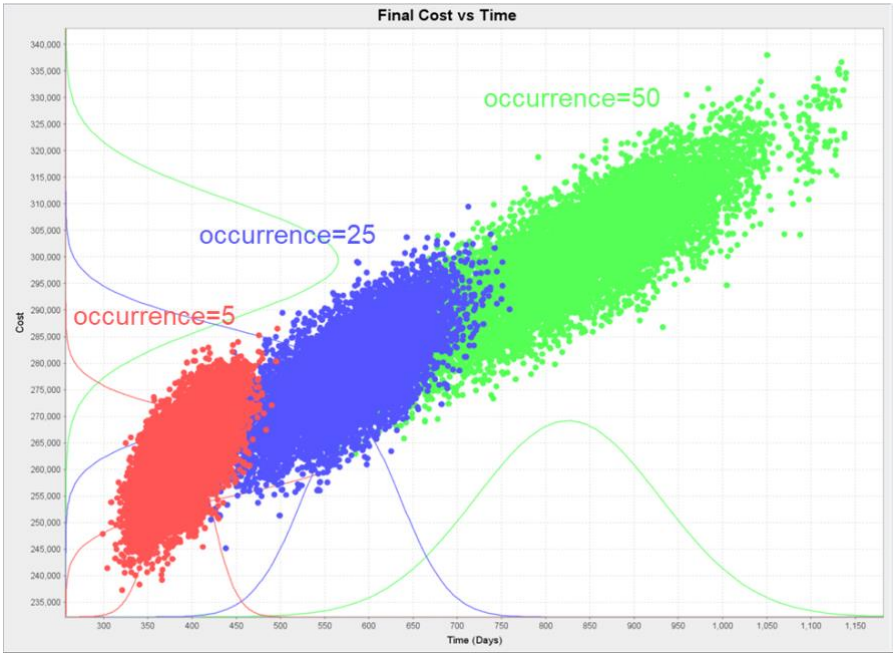

Figure 22 Sensitivity analysis on the number of water inflow occurrences

2.5.7.2 Proportion of water inflow

We also conducted a sensitivity analysis on the proportion of water inflow. This analysis specifically focuses on the scenario of small water inflow, as proportion only affects the small water inflow and number of occurrences affect primarily the large water inflows due to the delay and additional costs associated with catastrophic flows. The cost-time scattergram in Figure 23 illustrates the results of this sensitivity analysis.

During the analysis, we examined three different proportions of no inflow to inflow: 0.95/0.05, 0.9/0.1, and 0.8/0.2. The scattergram reveals that a higher proportion of inflow corresponds to increased time and cost, as the length of inflow increases. Additionally, a higher proportion of inflow results in a greater scatter of the results, indicating increased variability, and therefore risk.

It is important to note that compared to the number of occurrences, the proportion of inflow has a relatively smaller influence on the cost and time of construction. The number of occurrences remains a more significant factor in determining the additional cost and delay associated with water inflow.

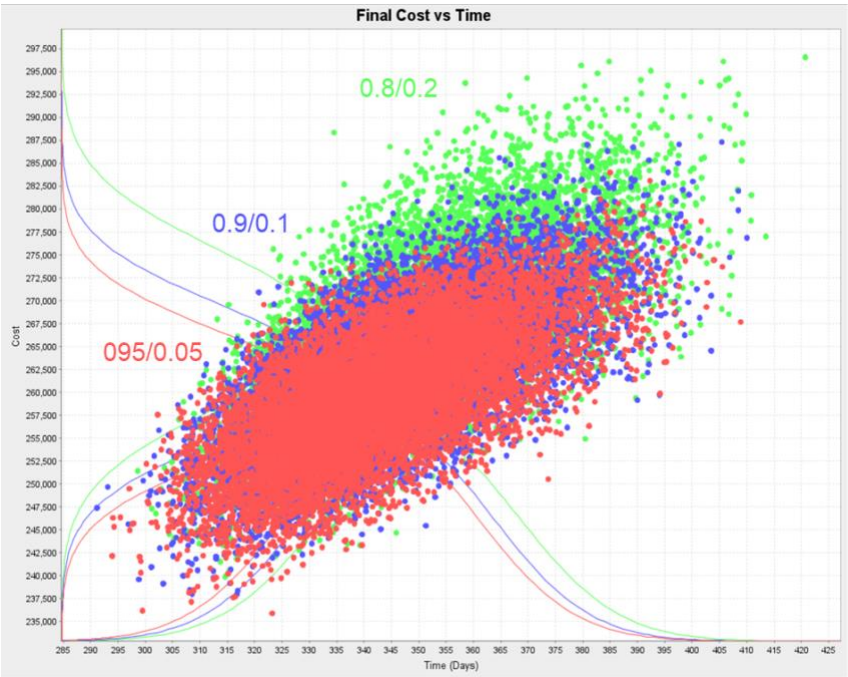

Figure 23 Sensitivity analysis of small water inflow proportion

2.5.7.3 Delay and additional cost

In addition to the sensitivity analyses conducted on the number of water inflow occurrences and the proportion of water inflow, we also investigated the values of delay and additional cost specifically for large water inflow. This sensitivity analysis excludes the small water inflow scenario as small water inflow does not imply delays and additional repair costs making this analysis irrelevant to this type of events. The investigated values are listed in Table 15, and the corresponding cost-time scattergram is shown in Figure 24.

The scattergram reveals that higher variability in the additional cost and delay leads to a greater scatter in the results, thus, greater risks. The increased variability can be observed as a wider spread of data points on the scattergram. It is important to note that the left edges of each scatter plot (origin) are the same since the minimum values are kept consistent across the different investigated values.

Table 15 cases of additional cost and delay investigated in the sensitivity analysis

Case		1	2	3
Additional cost	Min	250	250	250
	Mode	340	450	550
	Max	460	650	850
Delay	Min	5	5	5

	Mode	8	15	25
	Max	10	25	45

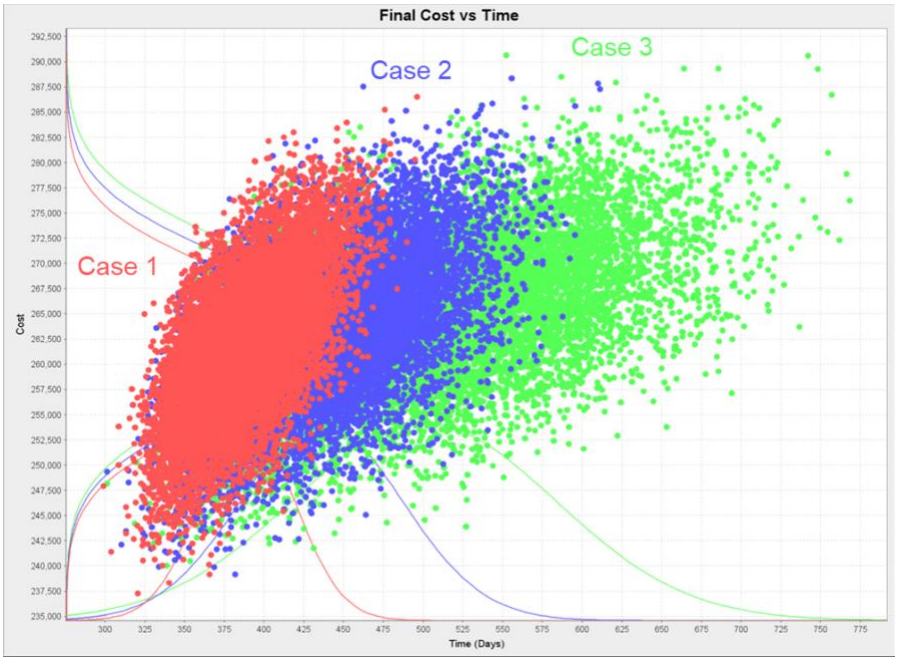

Figure 24 Sensitivity analysis of delay and additional cost

2.5.7.4 Increased cost and decreased advance rate

The sensitivity analysis of the values of increase in cost and decreased in advance rate in small water inflow scenarios provides insights into their impacts on tunnel construction time and cost. The examination of different values, as listed in Table 16, allows us to assess the variability in these parameters and its effect on the cost-time relationship.

The cost-time scattergram shown in Figure 25 illustrates that higher variability in advance rate and cost leads to increased scatter in the results. This indicates that variations in these parameters can influence the construction outcomes in terms of time and cost. It is important to note that despite the variations in these parameters, the minimum values remain the same for all studied cases, resulting in consistent lower boundaries for each scatter cloud.

Table 16 Variance of additional cost and delay

Case		1	2	3
Additional cost	Min	250	250	250
	Mode	340	450	550

	Max	460	650	850
Delay	Min	5	5	5
	Mode	8	15	25
	Max	10	25	45

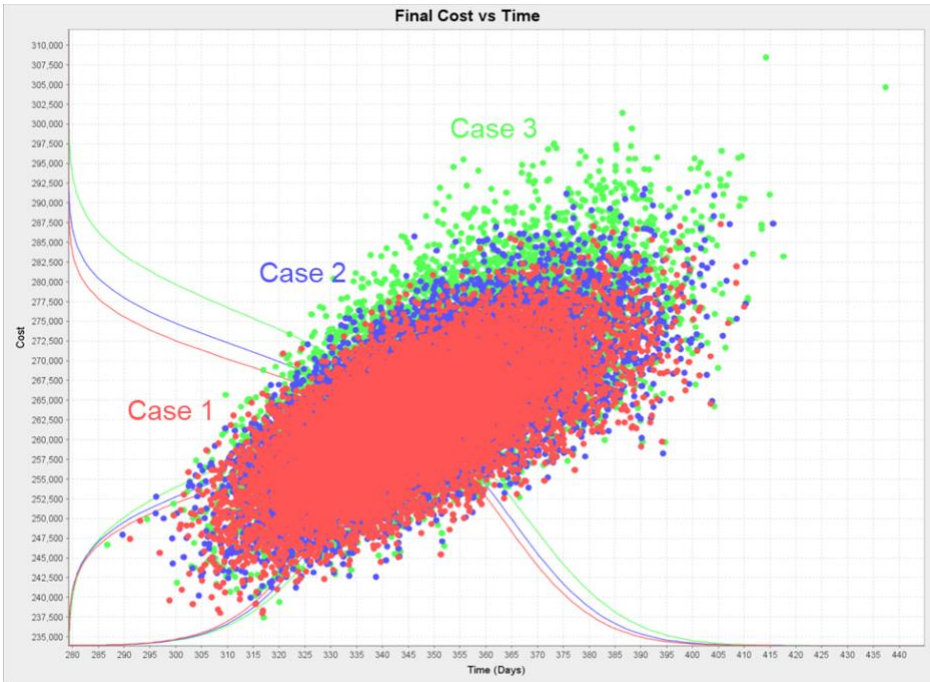

Figure 25 Sensitivity analysis of increased cost and decreased advance rate

The sensitivity results obtained from examining the impacts of parameters such as the number of water inflow occurrences, the proportion of inflow, delays and additional costs and the values of increased cost and decreased advance rate are significant in understanding the potential variations and uncertainties in tunnel construction. This knowledge can assist project planners and managers in making informed decisions, allocating appropriate resources, even gather more information on geology for example, and implementing suitable risk monitor and management strategies to address the potential cost and time implications associated with small and large water inflow events during tunnel construction.

2.6 Task 4 TBM advance rate prediction using machine learning (construction)

Advance rate prediction based on TBM sensor data has gained significant attention in recent years due to its potential for improving the efficiency and effectiveness of tunnelling projects. TBM

sensors capture valuable real-time information about the geological conditions, machine performance, and operational parameters during the excavation process. Leveraging this data through advanced predictive models can enhance the accuracy and reliability of advance rate estimation. The advance rate plays a critical role in calculating construction costs and timelines, as well as optimizing mechanized tunnelling performance. In this task we develop a ML model to predict advance rate based on TBM sensor data. These models can handle the complex relationships between sensor data and advance rate, capturing both local and global patterns, making them ideal to use in the context of tunneling. By training on historical data, ML models learn from past experiences and adapt predictions to varying project conditions. ML models excel in considering multiple factors simultaneously, incorporating geological characteristics, machine performance, operational settings, and environmental conditions. Furthermore, ML models can continuously learn and adapt by integrating real-time sensor data, enabling dynamic predictions and proactive adjustments to optimize tunnelling performance. This real-time feedback loop could empower operators and tunnelling engineers to make informed decisions, enhance productivity, and mitigate risks.

Because the Hudson tunnel was still on the planning phase, we used data from a TBM tunnel constructed in the city of Porto Portugal to build and demonstrate the model. We tested several ML algorithms (nearest neighbor (KNN), support vector regression (SVR), artificial neural networks (ANN), random forest (RF), and decision trees (DT) to determine the most suitable.

2.6.1 Brief data description

The monitored data are collected from the Porto light metro project line S in Porto, Portugal. This line is 3.95km long between the Salgueiros and Sao Bento stations (see Figure 26).

Figure 26 Plan view of Porto light metro project in Porto, Portugal

The excavation method adopted was an EPBM, a type of TBM , which is capable of both closed and open mode excavation in mixed face conditions. A thorough geological survey and

extensive site investigation (more than 500 boreholes) was done during the planning phase of the Porto Metro light metro project (70km long). Seven geomechanical groups have been defined, ranging from sound granite (g1 and g2) to saprolitic soil from granite (g5 and g6) and man-made material and alluvial deposits (g7) [19].

Tunnel of line S goes through ground conditions that ranged from saprolitic soil to sound granite, and all the intermediate alteration degrees. The groundwater level in the region is also very variable, and the tunnels run wholly beneath the water table. Another important feature of the subsurface of the city of Porto is the existence of so-called 'minas', a subsurface water distribution system of tunnels and galleries dating back to the 19th century which was not well charted at the time of the construction of the Porto Metro light rail, and thus posed an additional risk to the construction.

2.6.2 Feature Selection and Data preparation

The EPBM used in the Porto metro tunnel contained numerous sensors embedded in it which recorded a total of 195 features every 10 seconds, including data from both excavation and halt (e.g. segment assembly) phases of the tunnel construction. Since the focus of our work was to predict AR, only the data that corresponded to the excavation phase was included in the learning of the models, and all data corresponding to the halt phase was excluded. Also, parameters such as tank temperature, CH4-monitoring and gear oil tank level which are inconsequential to AR were excluded. Finally, based on previous research [20–23] and empiricism, a total of 9 parameters were selected as features for AR prediction, including torque cutting wheel, pressure force cutting wheel, thrust force, torque screw, cutting wheel speed of rotation, thrust pressure, excavated material flow, earth pressure, foam lance pressure.

For the sake of simplicity, these features and AR during one ring excavation (i.e., a length of 1.4m) was averaged. Furthermore, some variables, such as earth pressure and foam lance pressure, are measured by several sensors at different locations of the cutterhead (e.g. 7 sensors for earth pressure and 4 sensors for foam lance pressure). In this work, the average value of all earth pressure and the average value of all foam lance pressure sensor data was used for model development.

To fit each model and evaluate their prediction performance, 80% of the data were assigned randomly for training and 20% for testing of each model. Training data were divided into 4 folds for cross-validation and 1-fold was used for validation.

2.6.3 ML algorithms

Based on the summary of most commonly used ML algorithms [24,25], we chose five popular ML regression algorithms to use as foundation of our AR prediction models: KNN, SVR, ANN, RF, DT.

K-Nearest Neighbors regression (KNN) is a non-parametric method which, described in an intuitive manner, approximates the association between independent variables and the continuous outcome by averaging the observations in the same neighborhood [26].

Support Vector Regression (SVR) was developed for regression of datasets with high dimensions which are linearly non-separable. SVR is one of the most conventional approaches among ML techniques for regression since it reduces the prediction error as well as the complexity of the model [27].

Artificial neural networks (ANN) are a type of deep learning algorithm that simulates how the neurons in the human brain work. ANN consists of several layers composed of neurons. Each neuron is connected by synapses of other layers neurons. The synapses, or connected links, contain each an associated parameter (known as weights) which reflects the "strength" between the connected neurons. The transformation from input to output happens by the application of an activation function [28].

Random Forest (RF) is a group of decision trees. Random Forest Regression is a supervised learning algorithm that uses ensemble learning method to perform regression. Ensemble learning method is a technique that combines predictions from multiple machine learning algorithms to make a more accurate prediction than a single model [29].

Decision trees (DT), a nonparametric data mining technique, is an efficient statistical tool to develop prediction algorithms for a response variable [30].

2.6.4 Modeling results and analysis

The developed models' performance is presented in this section. The goodness of fit and model error was evaluated for each model using the coefficient of determination (R^2) and the root mean square error (RMSE). The results for each model's performance are summarized in Table 17.

Table 17 Performance of five different machine learning algorithms

Model	Training dataset (80%)		Testing dataset (20%)	
	R^2	RMSE	R^2	RMSE
KNN	0.877	3.634	0.837	3.216
SVR	0.946	1.560	0.911	1.745
ANN	0.865	3.987	0.795	4.033
RF	0.962	1.114	0.868	2.597
DT	0.881	3.526	0.771	4.521

For the training data, the R2 indicates that the developed models can explain 86.5-96.2% of AR variation using the selected features. Model error, expressed in RMSE, is low in all cases, ranging from 1.1-4.0, reinforcing the good performance of the models. The ranking of model performance in training data is: RF>SVR> DT> KNN> ANN. Testing data shows a relatively worse performance than the training data with R^2 varying from 77.1-91.1\% and RMSE from 1.7-4.5. The ranking of the model performance when it comes to the testing data is: SVR> RF> KNN > DT> ANN. As seen in Table 17, the SVR performed very well in both training and testing

with R2 of 94.6% and 91.1%, followed by RF, with R2 of 96.2% and 86.8%. While DT and ANN performed the worst when it comes to testing, with R2 of 77.1% and 79.5%, respectively.

Figure 27 shows the prediction output of each model versus the observed sensor data. The line $y=x$ means perfect prediction. In general, the results show that the developed models predicted AR in good agreement with the monitored AR. Most AR data lies in the range from 2 to 20 mm/min with about 20 points' values of AR range from 30 to 52 mm/min. For KNN and ANN model, good fitting for both training and testing data is shown in low values of AR (i.e., from 2 mm/min to 20 mm/min). However, for values of AR greater than that range, the model performance becomes worse and larger residual errors happen. This is reasonable as the amount of data points in the higher range values of AR is scarcer and not large enough to robustly train the model and therefore the predictions are worse in that range of AR. For SVR and RF, good performance is yielded for both low and high values of AR, showing that these models have a good ability to predict AR. RF shows a better fitting of the training data, yet a larger difference of R^2 between training and testing is observed in RF, i.e., a difference of 0.098 compared to 0.035 in SVR. This means that SVR may have a better predictive performance of AR than RF. Because of DT model's intrinsic characteristic which learns from data to approximately predict AR, predictions of DT model are neither smooth nor continuous, but stepwise constant approximations as seen in Figure 27e. Instead, a value would be used as a prediction for data in a specific range, which is the reason why predictions lie in a horizontal line, as seen in the plot. As a result, DT is not capable to capture the continuous nature of the AR sensor data.

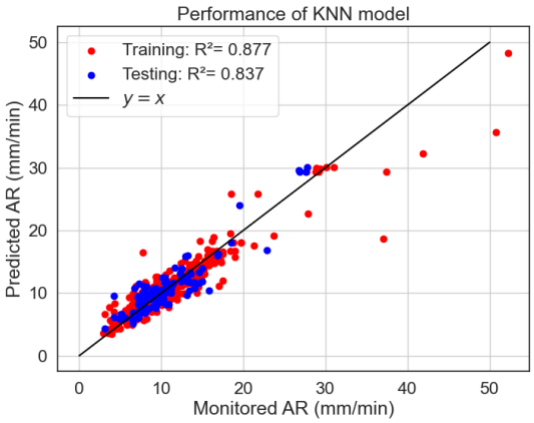

(a) KNN model

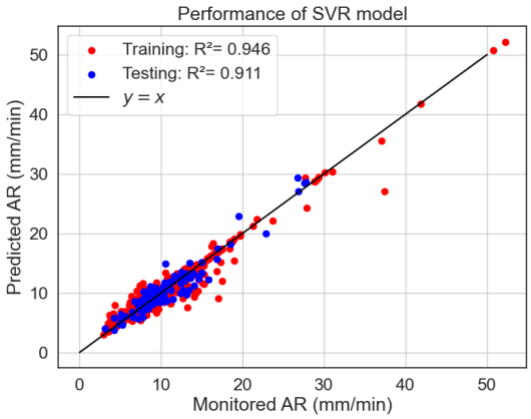

(b) SVR model

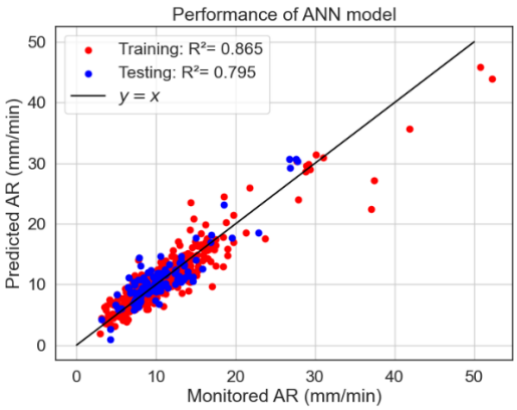

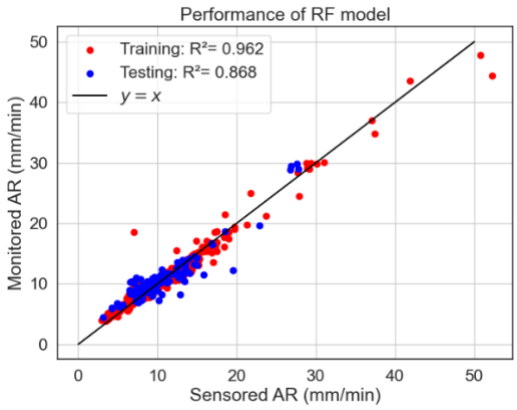

(c) ANN model (d) RF model

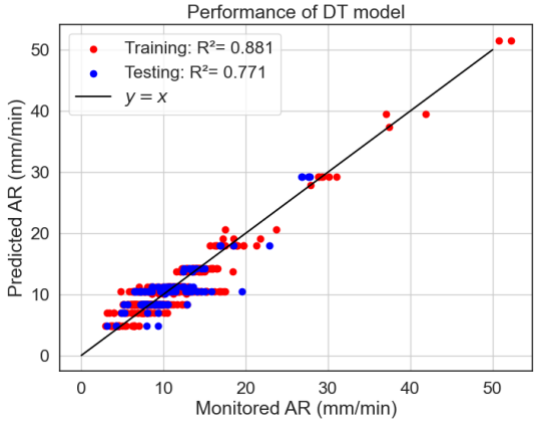

(e) DT model

Figure 27 Performance of five different ML algorithms

Plots of predicted and monitored AR as well as residual errors over all rings are plotted in Figure 28. Though large residual errors happen occasionally, close agreement between predicted and monitored AR can be observed in most of rings (as confirmed above), indicating that using these 9 features selected based on empiricism can capture the general trend of the monitored AR. Furthermore, the analysis of the residual errors reveals that errors mainly fluctuate around zero.

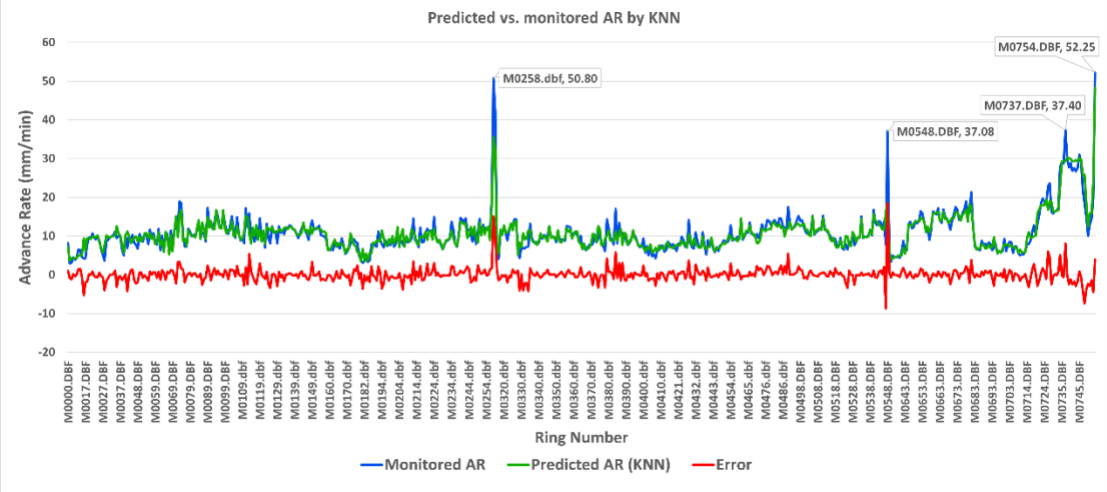

(a) KNN model

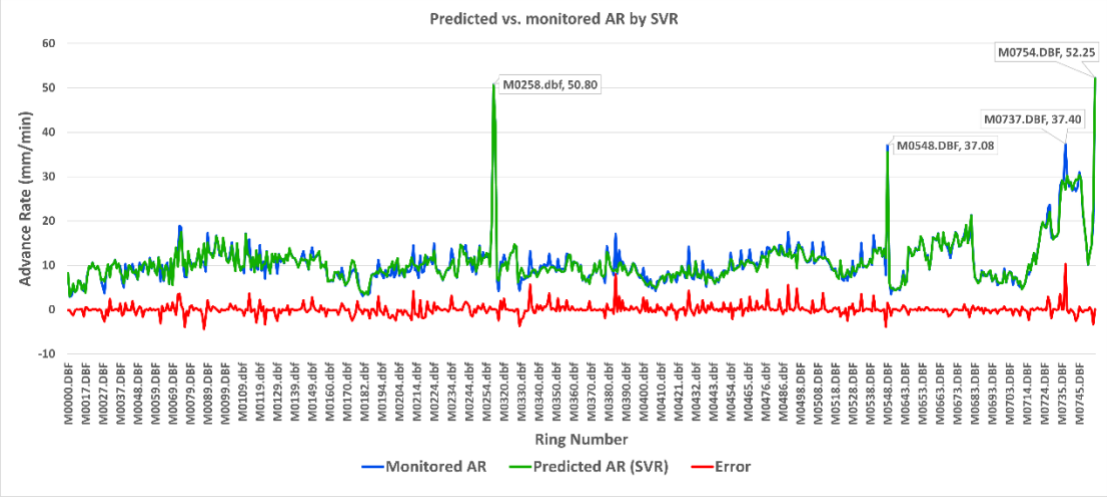

(b) SVR model

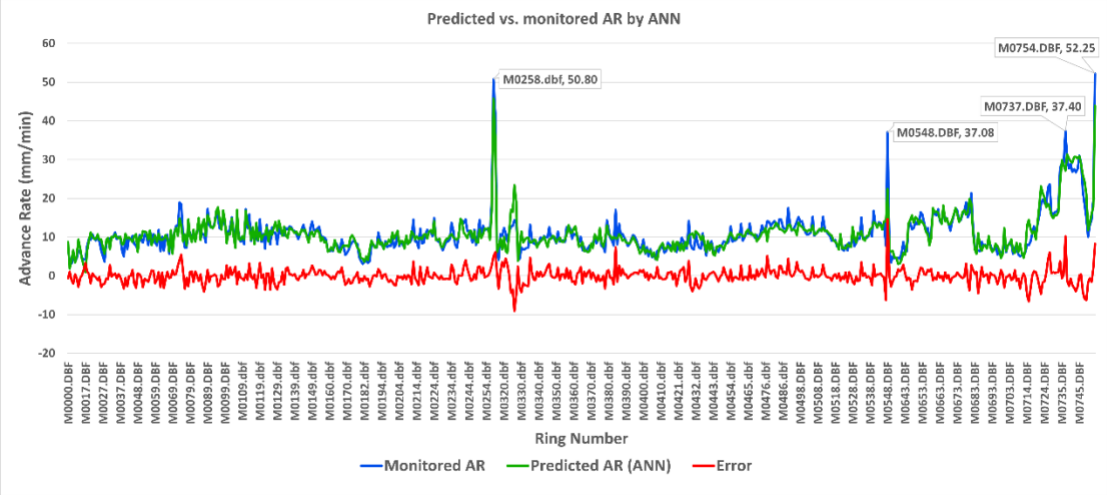

(c) ANN model

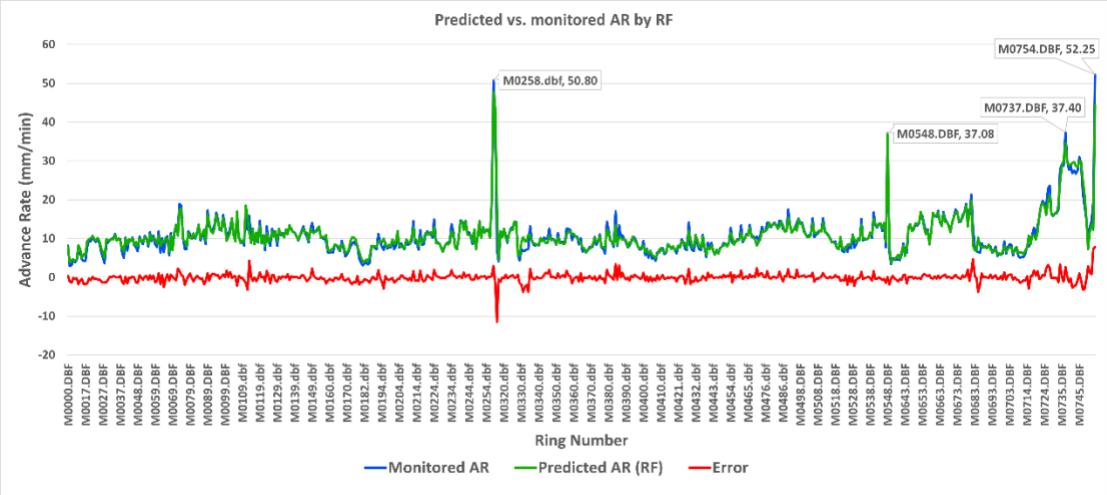

(d) RF model

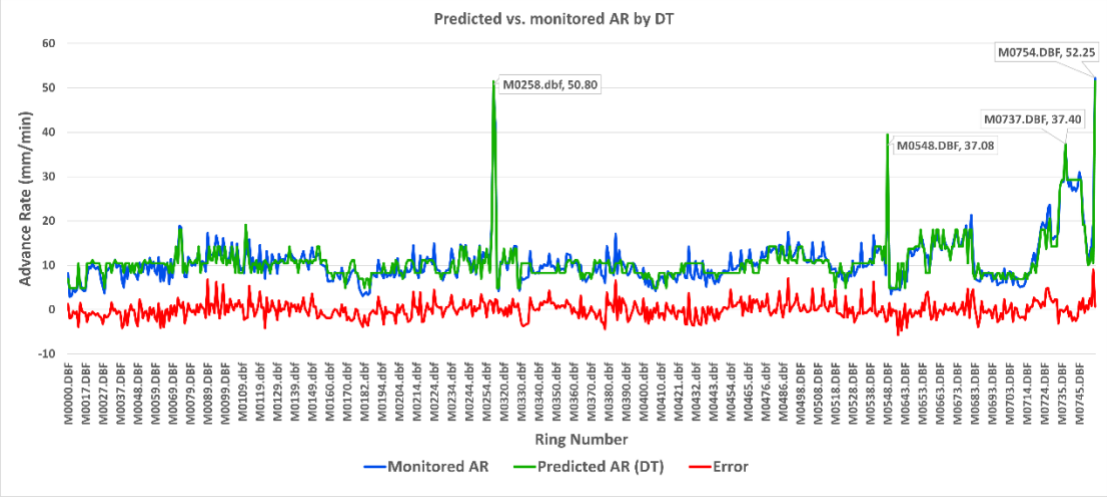

(e) DT model

Figure 28 Predicted AR, monitored AR, and residual errors over rings

Figure 28b and Figure 28d show that the residual errors for models SVR and RF have a stable trend, with small values and centered around zero, indicating the robust ability to predict AR. Figure 28c and Figure 28e show, for models ANN and DT, residual error trends are less stable than those observed in the SVR and RF models. Unusual large residual errors and abrupt differences in the AR sensor data can also be seen in the figures. These abnormal jumps in the AR sensor data values could indicate proximity to the portals, existence of obstructions, or change in geology and increased EPBM maintenance (e.g. cutter bit replacement).

Further exploration of residual errors (i.e., the differences between predicted and monitored AR) can provide valuable insights into the models' performance and underlying reasons for those large prediction errors. For this purpose, residual error distribution of all models is calculated and plotted in Figure 29. Mean (μ) and standard deviation (σ) characterize the distribution of errors, while 5th and 95th percentiles are calculated to show the extreme discrepancies. Kernel density estimation is shown in green line which presents the probability distribution of residual errors. Figure 29 reveals that residual errors, for all algorithms, are normally distributed with mean equals to zero. 5th and 95th percentiles also indicate that more than 90\% of the residual errors are less than 3 mm/min for most of the algorithms except DT.

The residual error distribution of SVR and RF are narrower compared to the ones of other algorithms which is consistent with the results shown in Table 17 and Figure 29. Besides, extreme residual errors can be observed from these histograms. Considering the randomness of models, it is not unusual for 1-2% of the points to have huge errors for no specific reason.

Hence, we will focus on the continuous error distribution. Absolute errors of DT can be as large as 7.5 mm/min, nearly 15% of the maximum AR of 50 mm/min. Absolute errors of KNN, ANN, and SVR are less than 6 mm/min, while the ones of RF are less than 5 mm/min. In addition, residual error distribution of DT shows a positive skew pattern, indicating that most of the outliers are overestimation of AR.

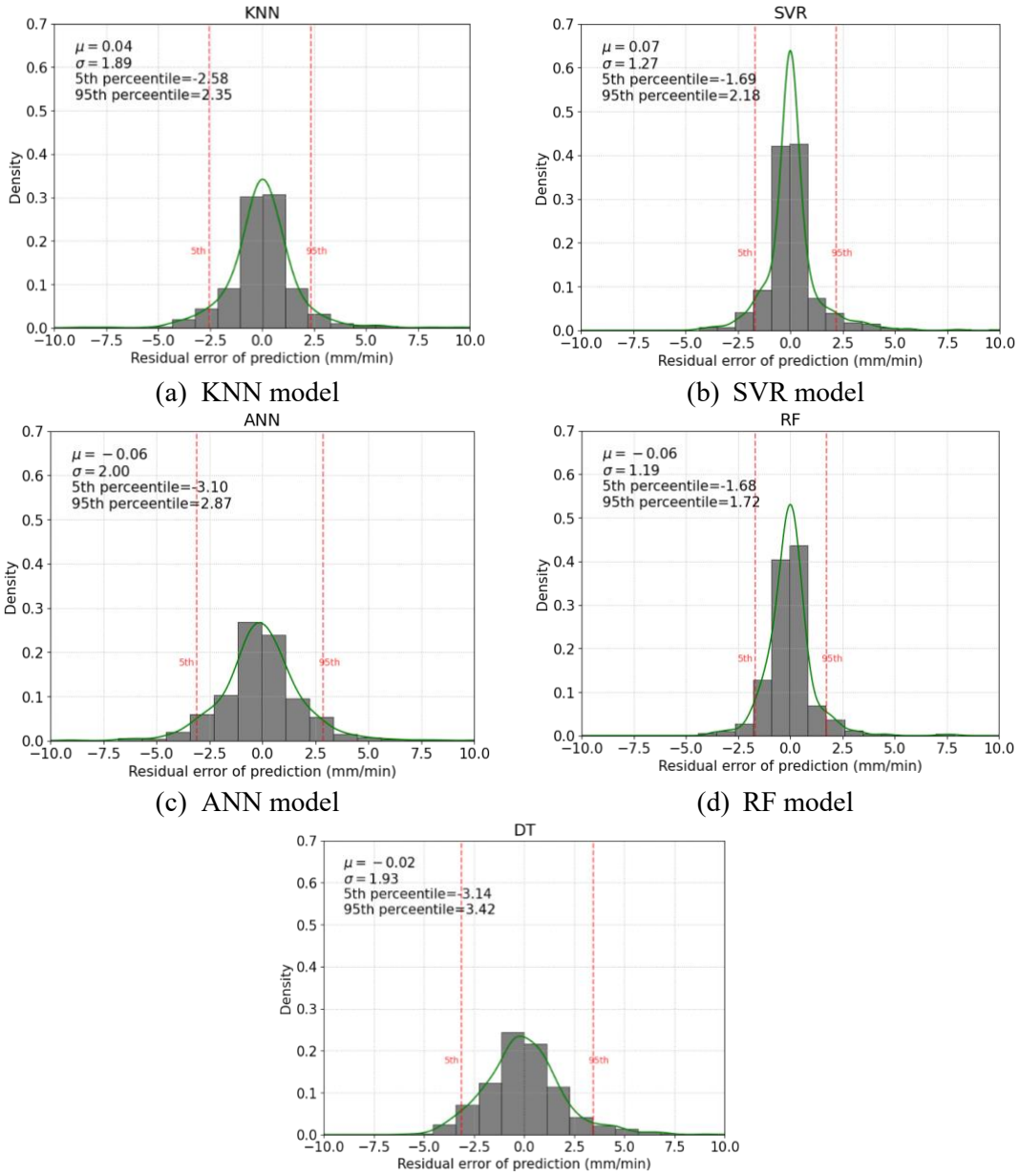

Figure 29 Residual error distribution of five machine learning algorithms

2.6.5 Analysis large AR and large residual errors

A further examination of the locations where large AR and large residual errors occurred can provide insight into our data and underlying causes of the observed predicted errors.

In Figure 30, rings where AR is "abnormal" (i.e., larger than the "typical" AR), can be observed. These AR large values seem to be outliers particularly when there is a large jump in the value of AR from one ring to another. Also, these anomalies in AR values may be biasing the models. There are, however, explanations for some of these values. For example, ring M0258 is

located at the entrance of a station where often a portal has been already constructed, and thus the soil (or most of it) has been removed. Often at these locations the EPBM is pulled through the already constructed shaft at the station location. This type of data can bias model fitting to some extent and is suggested to be excluded. Ring M0737 and M0754 are located where the geology transitions occur, from hard to soft ground conditions, and AR increased as most likely operator kept thrust pressure and torque screw unchanged. For ring M0548, no evidence was found as to why AR is so high at this location. Based on authors' experience, other reasons besides transition from hard to soft geological condition, could explain this raise: (1) maintenance: several cutter discs have been replaced just prior to the excavation of a ring; (2) encountering voids; (3) the existence of human made underground mines for water transport that are not chartered (the subsurface of Porto is known to have several). These large AR data should be treated carefully as they can induce bias in the model during training, particularly when data for training is limited.

In addition to large AR, there are some locations where residual errors are consistently large for several of the developed models, i.e., no model was able to accurately predict the performance of the machine through these locations. These are rings M0113, M0384 and M0726. Figure 30 and Figure 31 shows a comparison between the distribution of EPBM parameters (namely, torque cutting wheel, pressure force cutting wheel, thrust force, torque screw, cutting wheel speed of rotation, thrust pressure, excavated material flow, advance rate) for ring 384 (a large error ring) and ring 42 (a "normal" ring where prediction error is small), as an example.

In each figure, the values of the first two parameters correspond to the left y-axis while the last two correspond to the right one. It can be seen from these two figures that overall ring 42 shows a more stable trend compared to ring 384. AR varies greatly from 0 to 48 mm/min during the excavation of ring 384 while variation in ring 42 is smaller from 0 to 20 mm/min. In addition, during the excavation of ring 42 AR remains more "stable", while during the excavation of ring 384 there is a greater fluctuation, with the observation of at least two distinct zones. An initial zone where AR is quite high above 40mm/min, and a second zone with lower AR. The distinct behavior of the excavation in these two rings cannot be captured through the average of the ring data, which may be the source of some of the large observed residuals. The reason for the observed AR fluctuations is unknown, however one can observe that the rings where larger prediction errors occur, the sensor data tends to fluctuate more heavily than other rings. As averaged EPBM parameters are used, this unstable trend is inevitably not captured and may be preventing models from accurate prediction. Despite this, the models developed in this study presented very good predictions, it is suggested to investigate the use of time series data in modeling to better capture some of the changes that occur within the ring excavations.

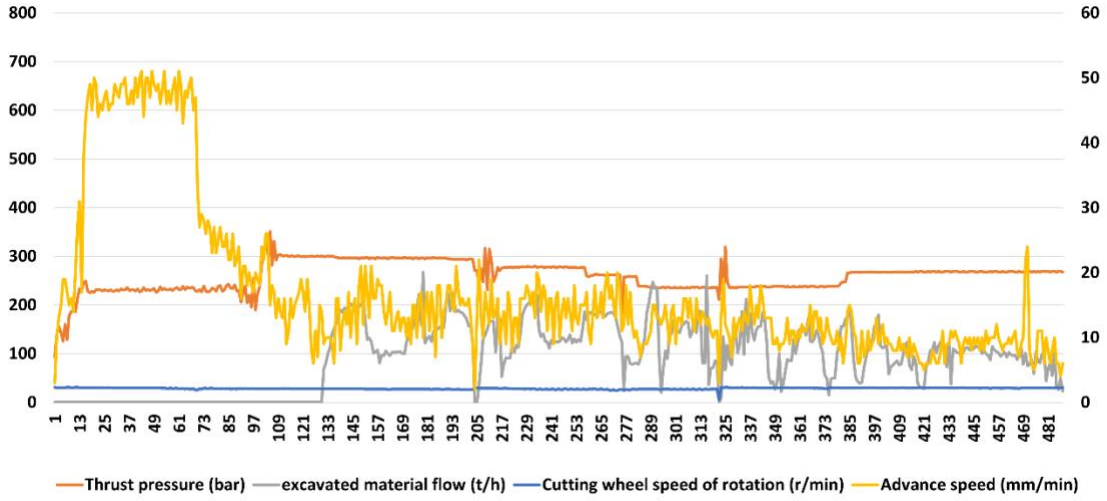

(a) Distribution of torque cutting wheel, pressure force cutting wheel, thrust force, torque screw

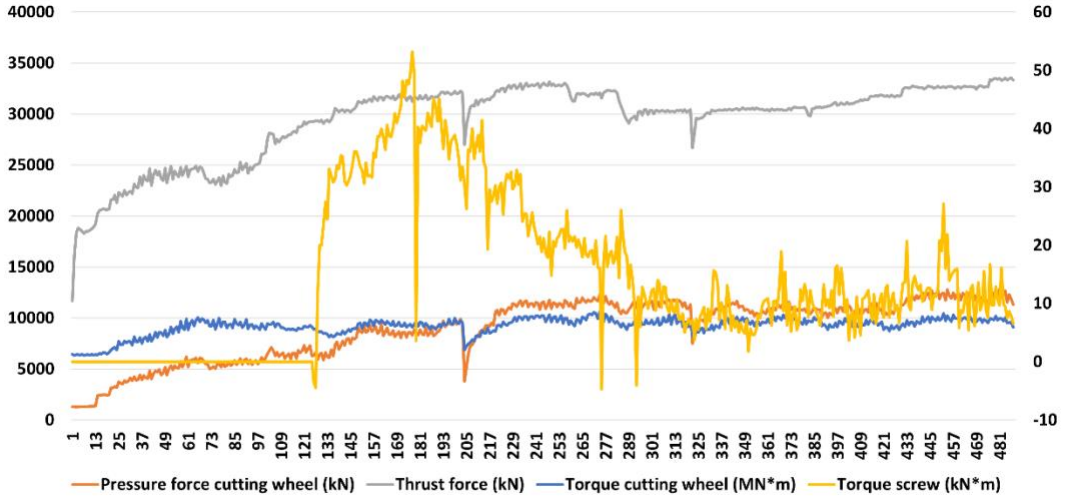

(b) Distribution of cutting wheel speed of rotation, thrust pressure, excavated material flow, advance rate

Figure 30 Distribution of features and label over ring 384

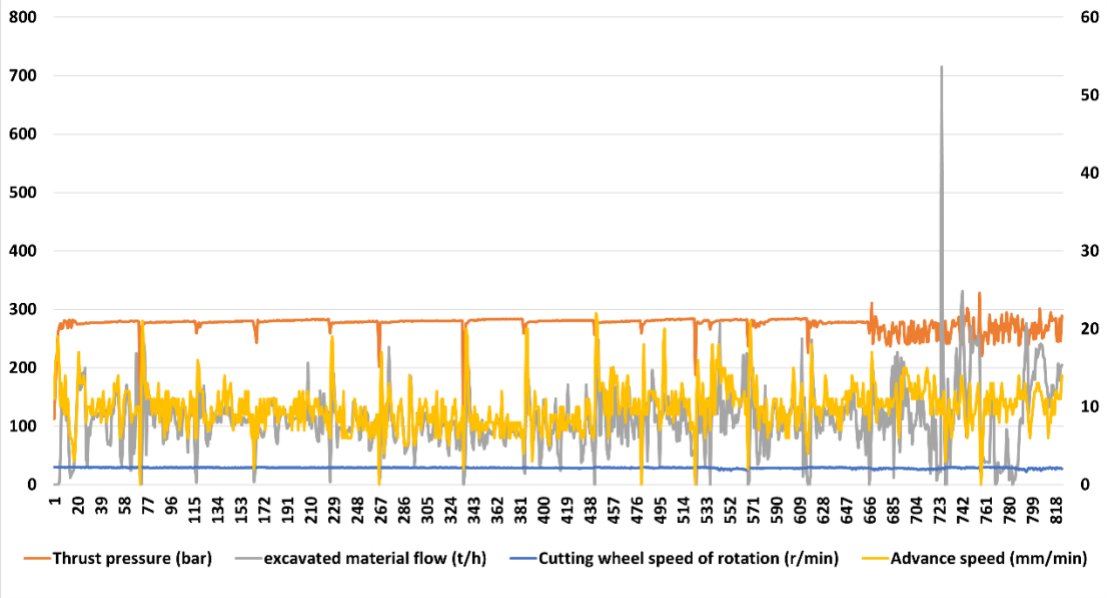

(a) Distribution of torque cutting wheel, pressure force cutting wheel, thrust force, torque screw

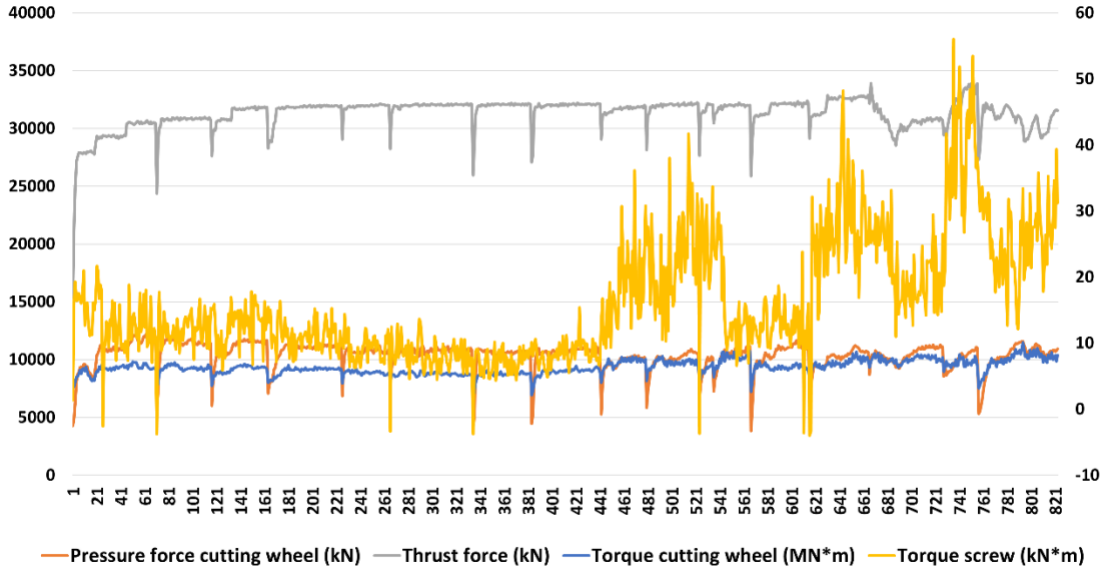

(b) Distribution of cutting wheel speed of rotation, thrust pressure, excavated material flow, advance rate

Figure 31 Distribution of features and label over ring 42

2.6.6 Validation against a different project

Most existing models are developed and validated against a single case study (one tunnel).

Given that the purpose of a prediction model is to make accurate predictions before (or during) construction, the ability to use these developed models to predict AR for other projects is of

extreme importance. We had the opportunity to gather data from two tunnels constructed in similar conditions (both using an EPBM) and in similar ground conditions (Porto Granite). Thus, to test the generalization ability of the developed models, we applied the models developed based on data from one tunnel - line S - to the other tunnel - line C - and tested their capability in predicting AR in a project with similar conditions. Line C tunnel shares similar geology with line S also in Porto and the same excavation method was used to build both tunnels. The predicted performance of the five models when applied to the new tunnel are shown in Figure 32. All models present underestimations of AR for line C. KNN model fitted the data poorly with a negative R^2 = -0.106, showing the worst performance among these 5 models. The ANN model, obtained a R^2 of only 0.033 which is near 0, implying that this model does not explain a lot of the variation in the AR. It is worth noting that even though SVR was the model that performed best in predicting AR of line S, the performance in AR prediction of line C is poor with R^2 of 0.077. RF and DT models showed relative better performance, with R^2 of 0.446 and 0.375, respectively. Of note is the fact that the geology is not considered as a feature in this study (only indirectly through machine parameters, which can be considered a reaction of the soil, and only 9 averaged features (machine parameters) were used, further research regarding the possibility of these models in predicting AR in another similar project will be done.

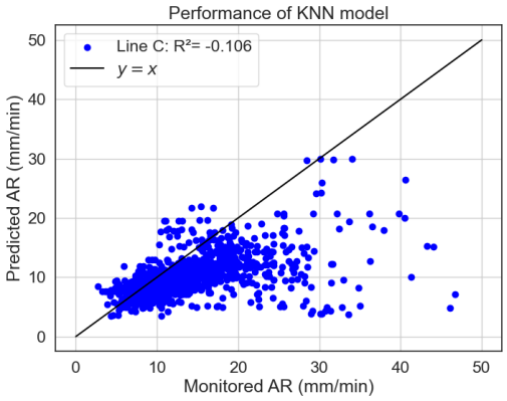

(a) KNN model

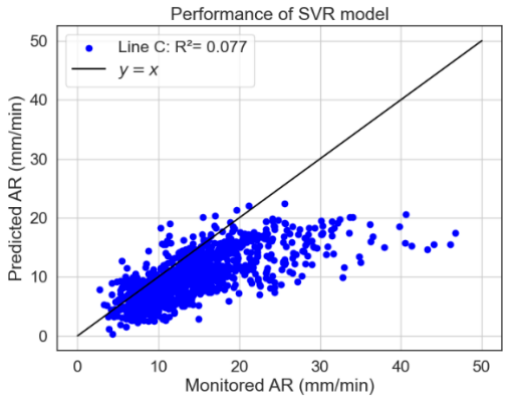

(b) SVR model

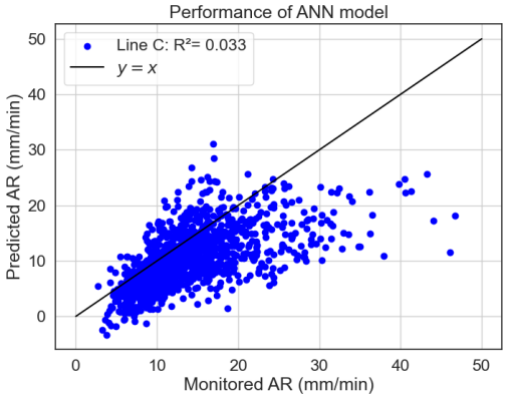

(c) ANN model

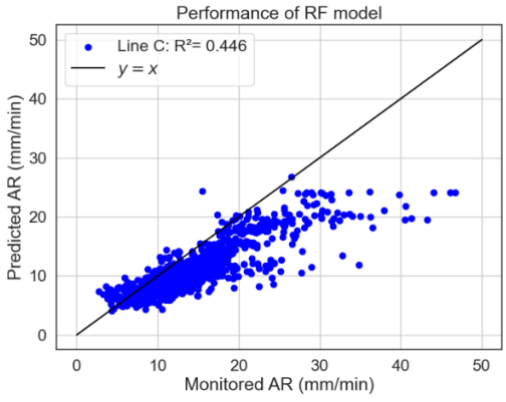

(d) RF model

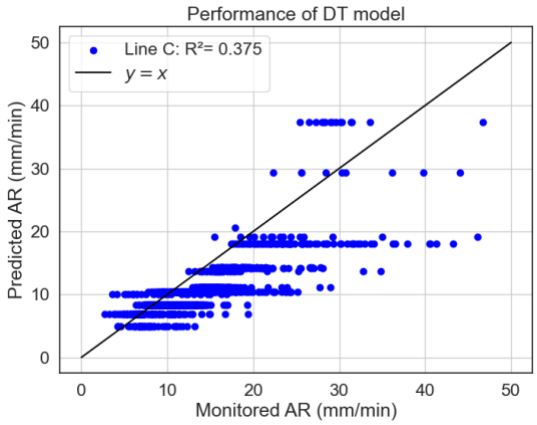

(e) DT model

Figure 32 Residual error distribution of five ML algorithms

Overall, the developed ML models demonstrated good performance in predicting advance rate based on TBM sensor data, with SVR and RF models showing the best results. These models have the potential to enhance the efficiency and effectiveness of tunnelling projects by providing accurate and dynamic predictions, empowering operators, and engineers to make informed decisions and optimize performance. However, further research and data collection are recommended to improve predictions, particularly for higher values of advance rate and outlier cases. Furthermore, it is important to emphasize the need for further research to apply models like the one discussed to other projects in different geologic conditions, such as the Hudson Tunnel. While the successful application of the model in the Porto project is promising, it does not guarantee similar results in every scenario.

3 Conclusions

The report presents a preliminary study of the Hudson Tunnel Project, focusing on the geologic and construction data collection, stochastic geologic modeling, risk characterization, quantification for planning, as well as advance rate forecast for Tunnel Boring Machine (TBM) during tunnel construction.

In the study, we developed a novel machine learning-based model to predict the lithology of the ground based on borehole data and applied it to the Hudson project data, which was instrumental in understanding the geological uncertainties related to the subsurface.

The initial geological study allowed us to identify areas of the tunnel that needed further in-depth study, and a detailed risk assessment. For that purpose, the Decision Aids for Tunnels (DAT) was adapted and customized to evaluate large-scale projects, such as the Hudson Tunnel. The DAT was instrumental in simulating geologies while considering uncertainties related to ground conditions and simulating construction through the geology profiles generated by the geology module, to generate probabilistic costs and times of construction and thus financial risk related to the tunnel construction. Due to time restrictions associated with the duration of the project, to test our framework, we focused on looking into the effects of a particular hazard, tunnel water inflow

during construction, and we considered two cases: nuisance flooding and catastrophic flooding to tunnel face instability.

Several sensitivity analyses were performed to assess the impact of different variables on costs and times of construction. The parameters examined included the number of water inflow occurrences, the proportion of inflow, delays, additional costs, and the values of increased cost and decreased advance rate. The sensitivity results obtained from examining the impacts of these parameters were significant in understanding the potential variations and uncertainties in tunnel construction. As an example, the sensitivity analysis on the number of water inflow occurrences during tunnel construction showed a significant impact in both time and cost of construction, due to the need for additional measures to manage the water inflow, such as pumping and drainage systems, and potential repair work for any damage caused by the water. Furthermore, the analysis showed that higher variability in the number of water inflow occurrences leads to increased scatter in the results, due to the uncertainty associated with the testament costs and downtimes. In conclusion, the results reinforce that robust management of the risk of water inflow occurrences is crucial in tunnel construction. This would include an accurate prediction of water inflow occurrences, adequate risk monitoring during construction, and contingency plans for unexpected water inflow events.

For the construction phase, we focused on developing a machine learning-based Penetration Rate (PR) forecast model that uses sensor data collected by the TBM as input. This type of model is crucial to predict TBM performance and estimate the construction time and cost of a TBM tunnel, and thus crucial for project planning and scheduling, by allowing project managers to set realistic timelines and better coordinate the various activities involved in the construction process.

In conclusion, this pilot work provided a comprehensive approach to managing uncertainties in large-scale tunneling projects like the Hudson Tunnel Project. The methodologies and tools developed in this study, including the stochastic geologic modeling framework, the DAT, and the PR forecast model, provide valuable insights and strategies for managing risks and uncertainties in tunnel construction. We believe these tools and resources can assist project planners and managers in making more informed decisions, allocating appropriate resources, and implementing suitable risk monitor and better risk management strategies.

4 Recommendations

Building on the findings of this report, the following recommendations are proposed.

Enhanced Geological Modeling

The geological could be further improved by incorporating additional data sources, such as geophysical survey data, and laboratory and field test results, including Cone Penetration Tests (CPTs) and Standard Penetration Tests (SPTs). This would enhance the accuracy of the geological model. The same framework used to develop the probabilistic geological models could then be employed to create probabilistic models and maps of geotechnical engineering properties, such as strength and deformability. This would provide a more comprehensive understanding of the

subsurface conditions and help in better predicting and identifying that may be encountered during tunnel construction and a more effective evaluation of hazards and risks.

Numerical Modeling

It is recommended to perform numerical modeling of the most critical section of the Hudson Tunnel, particularly the section where the cover is below 22 feet and where ground improvement treatment will be done. This modeling, potentially using finite element or finite difference software such as FLAC or RS2, will provide a comprehensive understanding of the structural integrity and potential vulnerabilities of the tunnel in this area. This should include an assessment of face collapse and flooding.

Ground treatment simulations

Once we have a solid understanding of the tunnel's structure and potential vulnerabilities through numerical modeling, we can then simulate different soil treatment options. These simulations should consider the potential for face collapse and water inflow identified in the numerical modeling stage. By comparing the potential outcomes and effectiveness of each treatment method, we can select the most suitable option for maintaining the stability of the tunnel and mitigating the risks identified in the numerical model.

Probability of Failures

To obtain the probability of failures of the tunnel face, the implementation of random fields, or conditional random fields would be crucial. These techniques allow us to consider uncertainties associated with ground engineering properties, such as strength properties and stiffness in the recommended numerical modeling.

Hazard function determination

The modeling work proposed above would work as a basis to determine the probability of instability and hazard in a more systematic and in-depth way. These results could be combined with historical data, statistical analysis, or expert judgment to build hazard functions (the probability of the hazard occurring as a function of time)

Extension of the work to other hazards

The work done and proposed in this report can be expanded to consider other hazards – e.g. seismic, landslides, soil erosion, and others.

Stakeholder Engagement

Due to the limited time and other constraints, the engagement with the stakeholder – gateway Cooperation – wasn't as frequent as desired. It would be beneficial to establish a more systematic approach to stakeholder engagement throughout the project lifecycle. This could involve regular communication, involvement in decision-making processes, and consideration of stakeholder inputs in risk assessment and management strategies.

Monitoring and Updating

Uncertainty management is an ongoing process. It's important to monitor the project and update the uncertainty assessment as new information becomes available (both design and construction). This could involve updating the models, revising the uncertainty quantification, or adjusting the uncertainty management strategies. We recommend that all the developed tools include an updating module to update predictions and risk assessment as the construction progresses.

Real-Time Monitoring System for TBM

The work done for Penetration Rate prediction based on TBM sensor data could be expanded to create and implement a comprehensive real-time monitoring system for the TBM. This system would track key parameters such as ground deformations, water pressure, changes in ground conditions, and stresses in the tunnel lining, providing early warning of potential problems and informing decision-making during construction.

References

[1] A.A. Drake Jr, R.A. Volkert, D.H. Monteverde, G.C. Herman, H.F. Houghton, R.A. Parker, R.F. Dalton, Bedrock geologic map of northern New Jersey, US Geological Survey, 1997.

[2] A.M. Lemon, N.L. Jones, Building solid models from boreholes and user-defined cross-sections, Comput Geosci. 29 (2003) 547–555.

[3] S. Adusumilli, D. Bhatt, H. Wang, P. Bhattacharya, V. Devabhaktuni, A low-cost INS/GPS integration methodology based on random forest regression, Expert Syst Appl. 40 (2013) 4653–4659.

[4] J. Zhou, X. Shi, K. Du, X. Qiu, X. Li, H.S. Mitri, Feasibility of random-forest approach for prediction of ground settlements induced by the construction of a shield-driven tunnel, International Journal of Geomechanics. 17 (2017) 4016129.

[5] L. Breiman, Random forests, Mach Learn. 45 (2001) 5–32.

[6] V.K. Singh, D. Singh, T.N. Singh, Prediction of strength properties of some schistose rocks from petrographic properties using artificial neural networks, International Journal of Rock Mechanics and Mining Sciences. 38 (2001) 269–284.

[7] P. Liashchynskyi, P. Liashchynskyi, Grid search, random search, genetic algorithm: a big comparison for NAS, ArXiv Preprint ArXiv:1912.06059. (2019).

[8] F. Pedregosa, G. Varoquaux, A. Gramfort, V. Michel, B. Thirion, O. Grisel, M. Blondel, P. Prettenhofer, R. Weiss, V. Dubourg, Scikit-learn: Machine learning in Python, The Journal of Machine Learning Research. 12 (2011) 2825–2830.

[9] A. Gulli, S. Pal, Deep learning with Keras, Packt Publishing Ltd, 2017.

[10] J. Bergstra, Y. Bengio, Random search for hyper-parameter optimization., Journal of Machine Learning Research. 13 (2012).

[11] D. Fourure, M.U. Javaid, N. Posocco, S. Tihon, Anomaly detection: how to artificially increase your f1-score with a biased evaluation protocol, in: Joint European Conference on Machine Learning and Knowledge Discovery in Databases, Springer, 2021: pp. 3–18.

[12] J. F. Pizzi, Geotechnical Data Report Palisades Tunnels and Hudson River Tunnels, 2018.

[13] R. Jia, Y. Lv, G. Wang, E. Carranza, Y. Chen, C. Wei, Z. Zhang, A stacking methodology of machine learning for 3D geological modeling with geological-geophysical datasets, Laochang Sn camp, Gejiu (China), Comput Geosci. 151 (2021) 104754.

[14] M. Hossin, M.N. Sulaiman, A review on evaluation metrics for data classification evaluations, International Journal of Data Mining & Knowledge Management Process. 5 (2015) 1.

[15] DEPARTMENT OF TRANSPORTATION, Hudson Tunnel Project Combined Final Environmental Impact Statement/Record of Decision and Final Section 4(f) Evaluation, Chapter 2, Federal Railroad Administration (FRA). (2021) 5–6.

[16] A.L. Costa, R.L. Sousa, H.H. Einstein, Probabilistic 3D alignment optimization of underground transport infrastructure integrating GIS-based subsurface characterization, Tunnelling and Underground Space Technology. 72 (2018) 233–241.

[17] H.H. Einstein, The Decision Acids for Tunnelling (DAT)-a brief review, Magazine of Korean Tunnelling and Underground Space Association. 3 (2001) 37–49.

[18] R. Harran, Decision Aids for Tunneling-A CATALOGUE FOR APPLICATION TO SMALL TUNNELS, 2018.

[19] S. Centis, G. Giacomin, EPB tunnelling in highly variable ground-the experience of Oporto Light Metro, in: TUNNELLING AND UNDERGROUND SPACE TECHNOLOGY. UNDERGROUND SPACE FOR SUSTAINABLE URBAN DEVELOPMENT. PROCEEDINGS OF THE 30TH ITA-AITES WORLD TUNNEL CONGRESS SINGAPORE, 22-27 MAY 2004, 2004.

[20] L. Rita, H.H. Sousa, Einstein. 2012, Risk Analysis during Tunnel Construction Using Bayesian Networks: Porto Metro Case Study. 27 (n.d.) 86–100.

[21] S. Mokhtari, M.A. Mooney, Predicting EPBM advance rate performance using support vector regression modeling, Tunnelling and Underground Space Technology. 104 (2020) 103520.

[22] Y. Pan, X. Fu, L. Zhang, Data-driven multi-output prediction for TBM performance during tunnel excavation: An attention-based graph convolutional network approach, Autom Constr. 141 (2022) 104386.

[23] J. Yang, S. Yagiz, Y.J. Liu, F. Laouafa, a comprehensive evaluation of machine learning algorithms on application to predict TBM performance, Undergr Space. (2021).

[24] S.K. Shreyas, A. Dey, Application of soft computing techniques in tunnelling and underground excavations: state of the art and future prospects, Innovative Infrastructure Solutions. 4 (2019) 1–15.

[25] B.B. Sheil, S.K. Suryasentana, M.A. Mooney, H. Zhu, Machine learning to inform tunnelling operations: recent advances and future trends, Proceedings of the Institution of Civil Engineers-Smart Infrastructure and Construction. 173 (2020) 74–95.

[26] J.K. Benedetti, On the nonparametric estimation of regression functions, Journal of the Royal Statistical Society: Series B (Methodological). 39 (1977) 248–253.

[27] H. Drucker, C.J. Burges, L. Kaufman, A. Smola, V. Vapnik, Support vector regression machines, Adv Neural Inf Process Syst. 9 (1996).

[28] M.S. Mhatre, F. Siddiqui, M. Dongre, P. Thakur, A review paper on artificial neural network: a prediction technique, Int J Sci Eng Res. 6 (2015) 161–163.

[29] G. Biau, Analysis of a random forests model, The Journal of Machine Learning Research. 13 (2012) 1063–1095.

[30] A. Mahmoodzadeh, M. Mohammadi, A. Daraei, H. Farid Hama Ali, A. Ismail Abdullah, N. Kameran Al-Salihi, Forecasting tunnel geology, construction time and costs using machine learning methods, Neural Comput Appl. 33 (2021) 321–348.